International Journal of Heat and Mass Transfer 115 (2017) 1206–1222

Contents lists available at ScienceDirect

International Journal of Heat and Mass Transfer

journal homepage: www.elsevier.com/locate/ijhmt

Review of spray cooling – Part 2: High temperature boiling regimes and quenching applications

Gangtao Liang [a,b], Issam Mudawar [b,*]

[a] Key Laboratory of Ocean Energy Utilization and Energy Conservation of Ministry of Education, School of Energy and Power Engineering, Dalian University of Technology, Dalian 116024, China
[b] Purdue University Boiling and Two-Phase Flow Laboratory (PU-BTPFL), School of Mechanical Engineering, 585 Purdue Mall, West Lafayette, IN 47907, USA

ARTICLE INFO

Article history:
Received 22 January 2017
Received in revised form 7 June 2017
Accepted 8 June 2017
Available online 26 June 2017

Keywords:
Spray cooling
Transition boiling
Film boiling
Leidenfrost point
Quenching

ABSTRACT

This paper is the second part of a comprehensive two-part review of spray cooling. The first part addressed the mechanisms and predictive tools associated with the relatively low-temperature single-phase liquid cooling and nucleate boiling regimes, as well as critical heat flux (CHF). The present part is focused on the relatively high-temperature transition boiling and film boiling regimes, and the Leidenfrost point. Discussed are dominant mechanisms, data trends, and predictive correlations and models. This information is especially important to the quenching of metal alloy parts from high initial temperature during heat treating. It is shown how correlations for the different spray cooling regimes and transition points can be implemented into boundary conditions for heat diffusion models to predict the temperature-time (quench) curve everywhere within the quenched part. It is also shown how the quench curve can be combined with the alloy's transformation kinetics to predict mechanical properties. By properly configuring the sprays used to quench complex-shaped parts, it is also possible to greatly enhance the mechanical properties while minimizing residual stresses.

© 2017 Elsevier Ltd. All rights reserved.

Contents

* Corresponding author.
E-mail address: mudawar@ecn.purdue.edu (I. Mudawar).
URL: https://engineering.purdue.edu/BTPFL (I. Mudawar).

http://dx.doi.org/10.1016/j.ijheatmasstransfer.2017.06.022
0017-9310/© 2017 Elsevier Ltd. All rights reserved.

Nomenclature

A	area defined along heated surface
A'	area defined along spherical surface centered at nozzle orifice
C_i	empirical coefficient
c_p	specific heat at constant pressure
C_t	critical time during quench
D	diameter of cylinder; inner diameter of tube
d	droplet diameter
d_{30}	volume mean droplet diameter
d_{32}	Sauter mean droplet diameter
G	mass flux
H	nozzle-to-surface distance; hardness
h_{fg}	latent heat of vaporization
k_i	constants in critical time relations
N^+	droplet number density
n_i	number of droplets with diameter d_i in sample
Nu	Nusselt number
P	pressure
ΔP	pressure rise
Pr	Prandtl number
Q	volumetric flow rate
Q''	local volumetric flux
q''	surface heat flux
$\overline{Q}''$	mean volumetric flux on surface
Q''_{dense}	volumetric flux corresponding to dense spray
R	universal gas constant
r	r coordinate
Re	Reynolds number
T	temperature
t	time
ΔT_{CHF}	surface-to-fluid temperature difference at CHF, $T_{w,CHF} - T_f$
ΔT_f	$T_w - T_f$
ΔT_{sat}	surface superheat, $T_w - T_{sat}$
ΔT_{sub}	liquid subcooling, $T_{sat} - T_f$
T_w^*	dimensionless surface temperature
u	droplet velocity
u_m	mean droplet velocity
u_{sound}	speed of sound in liquid
We	Weber number
x	x coordinate
x_i	number of droplets with diameter d_i
z	z coordinate

Greek symbols

β	angle in volumetric flux model
γ	angle in volumetric flux model
η	evaporation efficiency
θ	spray angle
μ	viscosity
ρ	density
σ	surface tension; yield strength
τ	quench factor
φ	half-angle of unit cell

Subscripts

CHF	critical heat flux
dense	dense spray
DFM	departure from film boiling
f	liquid
FW	film wetting regime
g	vapor
L	Leidenfrost temperature
max	maximum
MIN	minimum or Leidenfrost point
min	minimum
NB	nucleate boiling
s	spray
sat	saturation
sd	single droplet
ss	single droplet stream
sub	subcooling
TB	transition boiling
w	surface

1. Introduction

1.1. Spray cooling applications

1.1.1. Relatively high-flux, low temperature, steady-state cooling applications

As discussed in Part I of this study [1], there are two main types of applications of spray cooling. The first involves maintaining acceptable temperatures of heat-flux-controlled devices found in computers and data centers, X-ray medical devices, hybrid vehicle power electronics, heat exchangers for hydrogen storage, fusion reactor blankets, particle accelerator targets, magnetohydrodynamic (MHD) electrode walls, rocket nozzles, satellite and spacecraft electronics, laser and microwave directed energy weapons, advanced radars, turbine engines, and air-fuel heat exchangers in high-Mach aircraft [2]. Spray cooling in these applications is maintained mostly in the nucleate boiling regime safely below the critical heat flux (CHF) limit. The cooling is achieved in an appropriately configured spray chamber, which is incorporated into a closed two-phase flow loop. And, while both pressure and air-assist spray nozzles can tackle large heat loads, pressure nozzles are favored in most of these high-flux applications. These pressure nozzles employ only the momentum of the working liquid to achieve the droplet breakup, whereas air-assist nozzles require a secondary air stream to promote the breakup. Mixing air into the primary coolant greatly complicates flow loop operation, requiring specialized air separation equipment, and compromising both reliability and repeatability of cooling within the spray chamber.

Additionally, the cooling performance of air-assist nozzles is highly nozzle specific, especially in terms of spatial distribution of volumetric flux on the heated surface.

1.1.2. Relatively high temperature and transient cooling applications

A second type of applications is associated mostly with quenching of metal alloy parts from very high temperatures, often within the film boiling regime, in order to achieve optimal alloy microstructure and superior mechanical properties. Here, the temperature of alloy part is dropped rapidly to near room temperature, traversing the film, transition, nucleate boiling, and single-phase liquid cooling regimes.

As discussed in Part I [1], heat transfer performance of a spray can be described with aid of the boiling curve and/or the quench curve [3], which are shown in Fig. 4(a) and (b), respectively. The boiling curve is a representation of the variation of surface heat flux with surface superheat (surface temperature minus liquid saturation temperature), or surface-to-liquid temperature difference. A key advantage of the boiling curve is its effectiveness at displaying both the heat flux and wall temperature ranges associated with the different heat transfer regimes.

On the other hand, the quench curve, Fig. 4(b) in Part I, is a more effective representation of transient cooling behavior. Unlike the boiling curve, which is a measure of only surface effects, the quench curve is also highly influenced by thermal mass of the quenched part. The quench curve captures cooling rate variations in the form of substantial slope changes. The quench is initiated with slow cooling in the film boiling regime down to the Leidenfrost point, below which the cooling rate increases in the transition boiling regime, and reaches maximum in the nucleate boiling regime, before ultimately subsiding in the single-phase regime. The quench curve highlights the importance of the Leidenfrost point to materials processing applications since it marks the sharp transition from very slow cooling within the film boiling regime to much faster cooling in the transition boiling regime. As discussed latter in this paper, these changes in cooling rate, and the corresponding temperature ranges, have profound influences on microstructure and mechanical properties of a quenched metal alloy part.

1.2. Key spray parameters

As discussed in part I of this study [1], aside from thermophysical properties of the working fluid, key parameters that are used to correlate spray heat transfer data include: liquid initial temperature, T_f, liquid saturation temperature, T_{sat}, surface temperature, T_w, surface-to-fluid temperature difference, ΔT_f ($=T_w - T_f$), surface superheat, ΔT_{sat} ($=T_w - T_{sat}$), liquid subcooling ΔT_{sub} ($=T_{sat} - T_f$), mass flux, G, local volumetric flux, Q'', mean volumetric flux, $\overline{Q}''$, Sauter mean droplet diameter, d_{32}, and mean droplet velocity, u_m. Others include spray Reynolds number, Re, and Weber number, We, which are each defined in two different ways. Using mean volumetric flux as characteristic velocity, they are defined as

$$Re_s = \frac{\rho_f \overline{Q}'' d_{32}}{\mu_f} \tag{1a}$$

and

$$We_s = \frac{\rho_f \overline{Q}''^2 d_{32}}{\sigma}. \tag{1b}$$

And by replacing $\overline{Q}''$with u_m, they are defined as

$$Re_d = \frac{\rho_f u_m d_{32}}{\mu_f} \tag{2a}$$

and

$$We_d = \frac{\rho_f u_m^2 d_{32}}{\sigma}. \tag{2b}$$

1.3. Objectives of present review

This second part of a two-part review addresses the higher temperature spray cooling regimes, transition boiling and film boiling, as well as the Leidenfrost point, for pressure spray nozzles. The other lower temperature regimes, single-phase liquid cooling and nucleate boiling, and the CHF point, were discussed in detail in Part I [1]. The second objective of the present part is to address transient response of metal alloy parts as they are quenched from an initial high temperature down to room temperature. This part will also address the relationship between cooling rate and ultimate hardness and strength of the quenched part. These findings will be used to demonstrate the effectiveness of combining spray heat transfer correlations, volumetric flux distribution models, and metallurgical transformation theory to optimize the quenching of complex-shaped metal alloy parts in pursuit of both fast and uniform cooling, and superior mechanical properties.

2. Transition boiling

2.1. Heat transfer mechanisms

The transition boiling regime has historically received the least attention by investigators compared to all other spray cooling regimes. While transition boiling is known to consist of intermittent liquid contact with the surface and surface dryout, quantifying the ensuing transient heat transfer behavior is quite illusive. This regime is also difficult to measure using conventional steady-state heat-flux-controlled techniques. Additionally, development of an oxide layer on the surface has been reported to greatly influence heat transfer in this regime [4].

Both Toda [5] and Monde [6] found that the heat transfer coefficient increases with increasing spray volumetric flux. And Pais et al. [7] suggested that heat transfer can be enhanced by minimizing droplet size, maximizing droplet concentration, and using droplet velocities that minimize droplet rebound from the surface. Choi and Yao [8] reported that transition boiling performance for horizontal sprays is superior to that for vertical sprays, which is opposite to that in the film boiling regime.

Cui et al. [9] conducted experiments to investigate the influence of soluble salts on the water spray heat transfer in the transition boiling regime. Heat transfer performance was shown to be insensitive to the addition of NaCl or Na_2SO_4, but to improve with $MgSO_4$ because of increased roughness caused by adherence of $MgSO_4$ particles to the surface. Qiao and Chandra [10] noted that adding surfactant to the spray liquid slightly compromises heat transfer effectiveness during transition boiling because of suppression of heterogeneous bubble nucleation caused by a reduction in the liquid-solid contact angle.

2.2. Models and correlations

Mudawar and Valentine [11] noted a significant dependence of transition boiling data on the ratio u_m/Q'', and correlated heat flux in the transition boiling regime, q''_{TB}, to the critical heat flux, q''_{CHF}, and surface-to-fluid temperature difference at CHF, ΔT_{CHF} ($= T_{w,CHF} - T_f$),

$$\log_{10}\left(\frac{q''_{TB}}{q''_{CHF}}\right) = 4.78\times10^{5}\left(\frac{u_m}{Q''}\right)^{-1.255}\left[\log_{10}\left(\frac{\Delta T_f}{\Delta T_{CHF}}\right)\right]^3 - 1.90\times10^{4}\left(\frac{u_m}{Q''}\right)^{-0.903}\left[\log_{10}\left(\frac{\Delta T_f}{\Delta T_{CHF}}\right)\right]^2, \tag{3}$$

where

$$\Delta T_{CHF} = 18\left[\rho_g h_{fg} Q''\left(\frac{\sigma}{\rho_f Q''^2 d_{32}}\right)^{0.198}\right]^{1/5.55}. \quad (4)$$

Eqs. (3) and (4) are valid for d_{32} = 0.405–1.351 mm. They also recommended an alternative correlation based on $d_{0.5}$ as mean diameter,

$$\log_{10}\left(\frac{q''_{TB}}{q''_{CHF}}\right) = 1.90\times10^{5}\left(\frac{u_m}{Q''}\right)^{-1.144}\left[\log_{10}\left(\frac{\Delta T_f}{\Delta T_{CHF}}\right)\right]^{3} - 1.06\times10^{4}\left(\frac{u_m}{Q''}\right)^{-0.903}\left[\log_{10}\left(\frac{\Delta T_f}{\Delta T_{CHF}}\right)\right]^{2}, \quad (5)$$

where $d_{0.5}$ = 0.434–2.005 mm. The above general form of the q''_{TB} correlation was also adopted by Dou et al. [12], who used the spray Weber number instead of u_m/Q'',

$$\log_{10}\left(\frac{q''_{TB}}{q''_{CHF}}\right) = 4.6\times10^{6}We_s^{0.3}\left[\log_{10}\left(\frac{\Delta T_f}{\Delta T_{CHF}}\right)\right]^{3.36} - 3.3\times10^{6}We_s^{0.29}\left[\log_{10}\left(\frac{\Delta T_f}{\Delta T_{CHF}}\right)\right]^{3.28}, \quad (6)$$

which is valid for flow rates ranging from 30 to 50 l/min.

Later, Klinzing et al. [13] identified two distinct cooling regimes for water sprays based on local volumetric flux: low flux sprays for $Q'' < 3.5\times10^{-3}$ m^3 s^{-1}/m^2, and high flux sprays for $Q'' > 3.5\times10^{-3}$ m^3 s^{-1}/m^2. They correlated the transition boiling heat flux as

$$q''_{TB} = q''_{CHF} - \frac{q''_{CHF} - q''_{MIN}}{(\Delta T_{CHF} - \Delta T_{MIN})^3} \times\left[\Delta T_{CHF}^3 - 3\Delta T_{CHF}^2\Delta T_{MIN} + 6\Delta T_{CHF}\Delta T_{MIN}\Delta T_f - 3(\Delta T_{CHF} + \Delta T_{MIN})\Delta T_f^2 + 2\Delta T_f^3\right], \quad (7)$$

where q''_{MIN} and ΔT_{MIN} are, respectively, the heat flux and surface-to-fluid temperature difference corresponding to the Leidenfrost point, the latter is defined as $\Delta T_{MIN} = T_{w,MIN} - T_f$. Both q''_{MIN} and ΔT_{MIN} will be discussed later in Section 3.2. Eq. (7) is valid for Q'' = 0.6 × 10^{-3}–9.96 × 10^{-3} m^3 s^{-1}/m^2, u_m = 10.1–26.7 m/s, d_{32}= 0.405–1.35 mm, and T_f = 23 °C.

Bernardin and Mudawar [14] attempted to extrapolate the empirical heat transfer correlations for a single water droplet stream into a model for transition boiling heat flux for dilute sprays by accounting for hydrodynamic differences between a droplet stream and a spray,

$$q''_{TB} = \rho_f(h_{fg} + c_{p,f}\Delta T_{sub})\eta_{sd}(1 - Q''/Q''_{dense}) + 3.46\times10^{8}\Delta T_f^{-1.297}d_{32}^{-0.927}u_m^{-0.405}(Q''^2/Q''_{dense}), \quad (8)$$

where Q''_{dense} = 5 × 10^{-3} m^3 s^{-1}/m^2 and η_{sd} is the heat transfer efficiency of a single impinging droplet. This correlation is valid for ΔT_f = 100–220 °C, d_{32}= 0.25–1.002 mm, and u_d = 1.0–7.1 m/s, and is applicable to very dilute sprays ($Q'' \approx 0.5\times10^{-3}$ m^3 s^{-1}/m^2) and begins to lose accuracy for $Q'' > 1.0\times10^{-3}$ m^3 s^{-1}/m^2. Bernardin and Mudawar speculated that the limitation of Eq. (8) to dilute sprays is related to complex droplet interactions that take place in intermediate and dense sprays.

Liu et al. [15] developed a correlation for heat flux in both the nucleate boiling and transition boiling regimes for water sprays used in high pressure die casting,

$$\frac{q''_{TB\&NB}}{\rho_f\overline{Q}''h_{fg}} = C_1T_w^{*3} + C_2T_w^{*2} + C_3T_w^{*} + C_4, \quad (9)$$

where T_w^* is dimensionless surface temperature defined as

$$T_w^* = \frac{T_w c_{p,f}}{h_{fg}}, \quad (10)$$

and the coefficients in Eq. (9) are given by

$$C_1 = 10^{-4.054}Re_d^{1.451}We_d^{-1.279}(u_m/\overline{Q}'')^{0.864}, \quad (11a)$$

$$C_2 = -10^{-3.616}Re_d^{1.319}We_d^{-1.173}(u_m/\overline{Q}'')^{0.916}, \quad (11b)$$

$$C_3 = 10^{-3.642}Re_d^{1.215}We_d^{-1.093}(u_m/\overline{Q}'')^{0.949}, \quad (11c)$$

and

$$C_4 = -10^{-4.152}Re_d^{1.140}We_d^{-1.037}(u_m/\overline{Q}'')^{0.963}. \quad (11d)$$

The above correlation technique is valid for air pressures of 1–3 bar, water pressures of 0.8–3.8 bar, u_m = 14.1–18.8 m/s, d_{32} = 4.2–30.7 μm, and $\overline{Q}''$ = 0.0065–0.017 m^3 s^{-1}/m^2.

Overall, available transition boiling heat transfer information remains quite limited in terms of both dominant mechanisms and predictive tools. More research is therefore needed to address the complex influence of droplets interactions, as well as intermittent liquid contact with the surface and surface dryout.

3. Film boiling

3.1. Influencing parameters

It is widely accepted that spray volumetric flux is the key parameter that influences heat flux in the film boiling regime [16]. Bolle and Moreau [17,18] and Mizikar [19] suggested that the film boiling heat transfer coefficient for water sprays is fairly insensitive to surface temperature, a conclusion that contradicts those of Sasaki et al. [20] and Mzad and Tebbal [21]. Sasaki et al. reported that nozzle type, subcooling, and nozzle-to-surface distance have negligible influences on the heat transfer coefficient. However, Ubanovich et al. [22] and Reiners et al. [23] found that moving the nozzle closer to the surface increases the heat transfer coefficient for water sprays, but aggravates heat transfer non-uniformity across the surface. For example, the experiments by Reiners et al. showed a change of 2000 W/m^2 K in the heat transfer coefficient over a surface distance of 100 mm. Sharief et al. [24] and Schmidt and Boye [25] reported that the heat transfer coefficient for water sprays increases with increasing droplet velocity, but bears only weak dependence on droplet diameter. Ito et al. [26] reported that, for the same flow rate, the average heat transfer coefficient for a water spray with 5 MPa nozzle pressure is 2.8 times larger than that with 0.7 MPa pressure.

Experiments by Choi and Yao [8,27] revealed that a vertical downward-facing water spray provides better film boiling heat transfer performance than a horizontal spray because of secondary contact of splattered droplets for the former. This is similar to the conclusion drawn by Lin et al. [28] and Yoshida et al. [29] for the nucleate boiling regime. Lin et al. also found that film boiling performance for multi-nozzle FC-72 spray cooling is better for upward-facing sprays than for horizontal sprays. And Yoshida et al. found that upward-facing sprays are superior to downward-facing sprays.

Choi and Yao [8,27] found that the effect of droplet Weber number, We_d, Eq. (2b), on heat transfer in film boiling is mainly influenced by spray intensity or mass flux. They suggested that film boiling heat transfer for dilute sprays increases with increasing We_d, and is weakly dependent on We_d for high We_d. Yoshida et al. [29] found that, when We_d < 80, droplets rebound from the surface in the film boiling regime, and the influence of surface orientation is appreciable because of limited secondary impingement

for upward-facing sprays. While, for dense sprays, the heat transfer is less sensitive to We_d. Yao and Choi [30], who varied droplet velocity and droplet diameter of water sprays independently, arrived at a similar conclusion concerning the influence of We_d for light versus dense sprays.

However, different recommendations have been made concerning the boundary between light and dense sprays. In fact, studies by Yao and Choi [30], Delcorio and Choi [31], Deb and Yao [32], and Klinzing et al. [13] resulted in local liquid mass flux values for water sprays ranging from 0.2 to 3.5 kg s^{-1}/m^2, while Yoshida et al. [29] distinguished light and dense sprays based on a volumetric flux value of 7×10^{-4} m^3 s^{-1}/m^2 for water and 4×10^{-4} m^3 s^{-1}/m^2 for FC-72.

Kim et al. [33–36] investigated dilute water spray cooling in a series of studies. Kim et al. [33] divided the cooling heat transfer area into stagnation and wall-flow regions. In the stagnation region, they suggested that the local heat transfer coefficient is dictated by volumetric flux, while in the wall-flow region, the heat transfer coefficient is fairly constant, dependent on the flow rate. In a follow-up study, Kim et al. [34] found that the heat transfer coefficient for subcooled water liquid film flow on the surface is similar to that for turbulent single-phase heat transfer, and most of the heat flux is consumed by increasing the liquid temperature. Later, Kim et al. [35] examined the heat flux distribution when water spray droplets interact with the liquid film flowing along the surface, and concluded that presence of the flowing film can decrease the heat flux. In a more recent paper, Nishio and Kim [36] developed a model for the heat flux distribution, which accounted for both droplet rebound and sensible heat; the local heat flux was presented as the sum of contributions of droplet impact, induced air flow, and radiation.

3.2. Models and correlations

3.2.1. Polydispersed sprays

A polydispersed spray is defined as a spray with different droplet velocities and diameters, the values of which depend on the type of nozzle used. Mudawar and Valentine [11] correlated the heat flux for water sprays at the Leidenfrost point according to

$$\frac{q''_{MIN}}{\rho_g h_{fg} Q''} = 0.145 \left(\frac{u_m}{Q''}\right)^{0.834}. \tag{12}$$

However, Klinzing et al. [13] found that, while Q'' has a significant influence on film boiling for both light and dense water sprays, droplet velocity is important only for dense sprays. They characterized dilute sprays by negligible droplet interactions during impact with the surface, and dense sprays by significant droplet interactions that alter heat transfer dependence on the spray's hydrodynamic parameters. Klinzing et al. used Q'', u_m, and d_{32} to correlate film boiling heat flux, q''_{FB}, minimum (Leidenfrost) heat flux, q''_{MIN}, heat flux within the region of departure from film boiling (discussed below), q''_{DFB}, surface-to-fluid temperature difference at minimum heat flux, ΔT_{MIN}, and surface-to-fluid temperature difference at q''_{DFB}. Listed in Table 1, these correlations are valid for $Q'' = 0.6 \times 10^{-3}$–9.96×10^{-3} m^3 s^{-1}/m^2, $u_m = 10.1$–26.7 m/s, $d_{32} = 0.405$–1.35 mm, and $T_f = 23$ °C.

Included in Table 1 are correlations by Klinzing et al. for a transition point termed *departure from film boiling* (DFB) (see Fig. 4(b) in [1]), which is associated with onset of vapor film breakup as the wall temperature is decreased from the film boiling regime. A *film wetting regime* (FW), associated with intermittent wetting and reformation of the vapor blanket, occurs between the DFB and Leidenfrost points. Klinzing et al. correlated the heat flux in the film wetting regime according to

$$q''_{FW} = C_0 + C_1 \Delta T_f + C_2 \Delta T_f^2, \tag{13}$$

where

$$C_0 = q''_{MIN} - C_1 \Delta T_{MIN} - C_2 \Delta T_{MIN}^2, \tag{14a}$$

$$C_1 = -2 C_2 \Delta T_{MIN}, \tag{14b}$$

and

$$C_2 = \frac{q''_{DFB} - q''_{MIN}}{\left(\Delta T_{DFB} - \Delta T_{MIN}\right)^2}. \tag{14c}$$

Yao and Choi [30] suggested that film boiling heat flux for water sprays bears a power-law dependence on liquid mass flux, and this relationship is somewhat stronger at low mass fluxes. For a droplet diameter of 0.46 mm, droplet velocities of 2.8–3.4 m/s, and mass fluxes of 0.0091–0.21 g s^{-1}/cm^2, the film boiling heat flux for water was correlated as

$$q''_{FB} = 170 G^{0.76}. \tag{15}$$

Al-Ahmadi and Yao [37] found that q''_{MIN} also depends on G,

$$q''_{MIN} = 161.6 G^{0.64}, \tag{16}$$

where $G = 1.5$–30 kg s^{-1}/m^2. Hsieh et al. [38] investigated film boiling of water and R-134a sprays using a transient liquid crystal technique, and recommended the following correlation for the Leidenfrost point:

$$q''_{MIN} = 0.11 h_{fg} \rho_g \left[\frac{\sigma g (\rho_f - \rho_g)}{(\rho_f + \rho_g)^2}\right]^{1/4}, \tag{17}$$

which is independent of droplet velocity.

Wendelstorf et al. [39] showed that the film boiling heat transfer coefficient for water sprays decreases with increasing wall-to-fluid temperature difference for $G > 10$ kg s^{-1}/m^2 and $\Delta T_f > 800$ °C, and recommended the correlation

$$h = 190 + \tanh\left(\frac{G}{8}\right)\left\{140G\left(1 - \frac{G\Delta T_f}{72{,}000}\right) + 3.26\Delta T_f^2\left[1 - \tanh\left(\frac{\Delta T_f}{128}\right)\right]\right\}, \tag{18}$$

which is valid to $3 < G < 30$ kg s^{-1}/m^2 and $\Delta T_f > 180$ °C. Fujimoto et al. [40] reported that the heat transfer coefficient for water can be correlated with droplet volume mean diameter, d_{30}, mean velocity, u_m, and number density of droplets, N^+

$$h = 1.90 d_{30}^{1.1} u_m^{1.1} N^{+0.65}, \tag{19}$$

where

$$d_{30} = \left(\frac{\sum_i n_i d_i^3}{\sum_i n_i}\right)^{1/3} \tag{20a}$$

and

$$u_m = \frac{\sum_i u_i d_i^3}{\sum_i d_i^3}, \tag{20b}$$

as shown in Fig. 1. Eq. (19) is valid for $d_{30} = 0.083$–0.206 mm, $u_m = 6.8$–15.6 m/s, and $N^+ = 3.77 \times 10^7$–1.48×10^8 m^{-3} (or $Q'' = 2.5 \times 10^{-4}$–2.18×10^{-3} m^3 s^{-1}/m^2).

3.2.2. Monodispersed sprays

Several investigators attempted to derive predictive tools for spray cooling by modifying models and correlations originally developed for a single droplet or a single droplet stream. Moriyama et al. [41] developed an analytical model for the local film boiling

Table 1
Summary of film boiling heat transfer correlations for water sprays [13].

	Low spray flux ($Q'' < 3.5 \times 10^{-3}$ m^3 s^{-1}/m^2)	High spray flux ($Q'' > 3.5 \times 10^{-3}$ m^3 s^{-1}/m^2)
q''_{FB}	$q''_{FB} = 63.25\Delta T_f^{1.691} Q''^{0.264} d_{32}^{-0.062}$	$q''_{FB} = 1.413 \times 10^5 \Delta T_f^{0.461} Q''^{0.566} u_m^{0.639}$
q''_{MIN}	$q''_{MIN} = 3.324 \times 10^6 Q''^{0.544} u_m^{0.324}$	$q''_{MIN} = 6.069 \times 10^6 Q''^{0.943} u_m^{0.864}$
q''_{DFB}	$q''_{DFB} = 6.100 \times 10^6 Q''^{0.588} u_m^{0.244}$	$q''_{DFB} = 6.536 \times 10^6 Q''^{0.995} u_m^{0.924}$
ΔT_{MIN}	$\Delta T_{MIN} = 2.049 \times 10^2 Q''^{0.066} u_m^{0.138} d_{32}^{-0.035}$	$\Delta T_{MIN} = 7.990 \times 10^3 Q''^{-0.027} u_m^{1.033} d_{32}^{0.952}$
ΔT_{DFB}	$\Delta T_{DFB} = 2.808 \times 10^2 Q''^{0.087} u_m^{0.110} d_{32}^{-0.035}$	$\Delta T_{DFB} = 3.079 \times 10^4 Q''^{-0.194} u_m^{1.922} d_{32}^{1.651}$

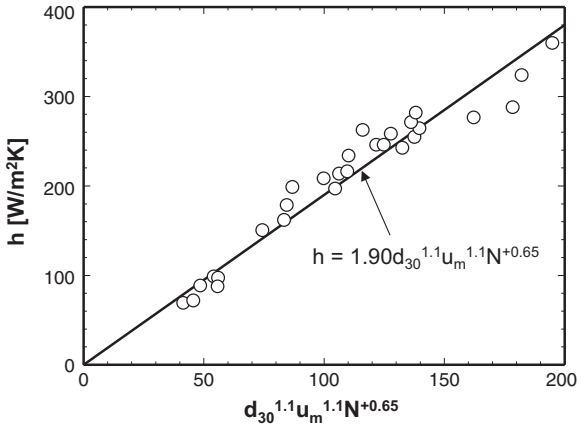

Fig. 1. Correlation of heat transfer coefficient in the film boiling regime. Adapted from Fujimoto et al. [40].

heat transfer coefficient for a spray based on an empirical relation for a single impinging droplet, which was corrected for spray volumetric flux, droplet diameter, and droplet velocity distribution. However, this model showed poor predictions of spray data, a weakness that can be attributed to velocity limitations of the single droplet model, and failure to account for droplet interference within a spray. Deb and Yao [32] constructed an analytical model for heat transfer for a spray with uniform droplet diameter and velocity, by accounting for droplet contact heat transfer, bulk air convection, and radiation. They represented the droplet contact heat transfer by a semi-empirical correlation for heat transfer effectiveness originally developed for single droplets. For dilute sprays, the model exhibited fair agreement with experimental data well into the film boiling regime, but significant error around the Leidenfrost point. In follow-up work by Deb and Yao [42], a dense spray model was formulated by a combination of asymptotic conditions of their earlier dilute spray model and a pool boiling model; the latter represents extreme surface flooding conditions of a dense spray. Film boiling showed very weak dependence on droplet parameters for dense sprays compared to strong dependence for dilute sprays. Delcorio and Choi [31] developed models for film boiling heat transfer in dilute and dense sprays using a sub-model for sensible heat exchange of single impinging droplets, by accounting for spray droplet number density and reduction in liquid-solid contact area resulting from multi-droplet interference. The dilute spray model showed fair agreement with experimental data, while the dense spray model exhibited substantial prediction errors.

By accounting for fundamental differences between a spray and an isolated droplet stream resulting from droplet interference, Bernardin and Mudawar [43] proposed a technique to predict film boiling heat transfer for light sprays. They recommended a local spray flux value corresponding to transition from light to dense water sprays of $Q''_{dense} = 5 \times 10^{-3}$ m^3 s^{-1}/m^2, and developed a relationship for heat transfer efficiency of a spray, η, in terms of efficiencies of a single water droplet, η_{sd}, and a single water droplet stream, η_{ss}, using linear interpolation based on Q''/Q''_{dense},

$$\eta = \eta_{sd} - \frac{Q''}{Q''_{dense}}(\eta_{sd} - \eta_{ss}). \tag{21}$$

They then extrapolated the correlation for a single droplet stream heat transfer rate to predict the film boiling heat flux and heat transfer efficiency for dilute sprays,

$$q''_{FB} = \rho_f(h_{fg} + c_{p,f}\Delta T_{sub})\eta_{sd}(1 - Q''/Q''_{dense}) + 1720\Delta T_f^{0.912} d_{32}^{-1.004} u_m^{-0.746}(Q''^2/Q''_{dense}) \tag{22a}$$

and

$$\eta = \frac{63.25}{\rho_f(h_{fg} + c_{p,f}\Delta T_{sub})}\Delta T_f^{1.691} Q''^{-0.736} d_{32}^{-0.062}. \tag{22b}$$

Notice that, because Eqs. (22a) and (22b) are derived from an empirical correlation for a single droplet stream, this model is better suited for the same operating conditions of the single stream data, namely, ΔT_f = 180–380 °C, d_{32} = 0.25–1.002 mm, and u_m = 1.0–7.1 m/s. However, the model is not suitable for dense sprays involving complex droplet interference effects.

Cox and Yao [44] examined film boiling heat transfer for monodispersed water sprays with large droplet diameters of 3–25 mm. Results showed that the spray heat flux has a strong power-law dependence on mass flux, while heat transfer efficiency for the film boiling regime, which they defined as

$$\eta = \frac{q''_{FB}}{G(h_{fg} + c_{p,f}\Delta T_{sub} + c_{p,g}\Delta T_{sat})} \times 100\%, \tag{23}$$

was proportional to $d^{-1/2}$, but independent of droplet velocity. Later, Yao and Cox [45] suggested using G/ρ_f instead of droplet velocity to define droplet Reynolds and Weber numbers to improve the accuracy of empirical correlations. They explored the variations of heat transfer efficiency with respect to both droplet Weber number, $We_d = \rho_f u_m^2 d_{32}/\sigma$, and spray Weber number, $We_s = \rho_f \overline{Q}''^2 d_{32}/\sigma$, using data from Yao and Choi [30], Choi and Yao [8], Ito et al. [46], Shoji et al. [47], and Cox and Yao [44], spanning mass fluxes of 0.016–2.05 kg s^{-1}/m^2, droplet velocities of 0.6–7.3 m/s, and droplet diameters of 0.13–25 mm. Given the larger scatter in the variation of η relative to We_d, Fig. 2(a), compared to that relative to We_s, Fig. 2(b), they suggested adopting We_s in correlations to achieve better predictive accuracy. Using this rationale, they recommended the following correlation for heat transfer efficiency in film boiling:

$$\eta = 8 \times 10^{-7}\left(\frac{We_s T_{sat}}{\Delta T_f}\right)^{-0.62} + 3.5 \times 10^{-3}\left(\frac{We_s T_{sat}}{\Delta T_f}\right)^{-0.2}, \tag{24}$$

which is valid for $6 \times 10^{-10} < We_s < 3 \times 10^{-2}$. Yao and Cox suggested several reasons for the monotonic decline of η with increasing We_s. First, an increase in We_s increases the impact intensity of the spray droplets and the droplet collisions, which reduces the effective heat transfer area and momentum of individual droplets. Second, high We_s values are associated with large mass fluxes, which promote surface flooding, meaning the droplets lose

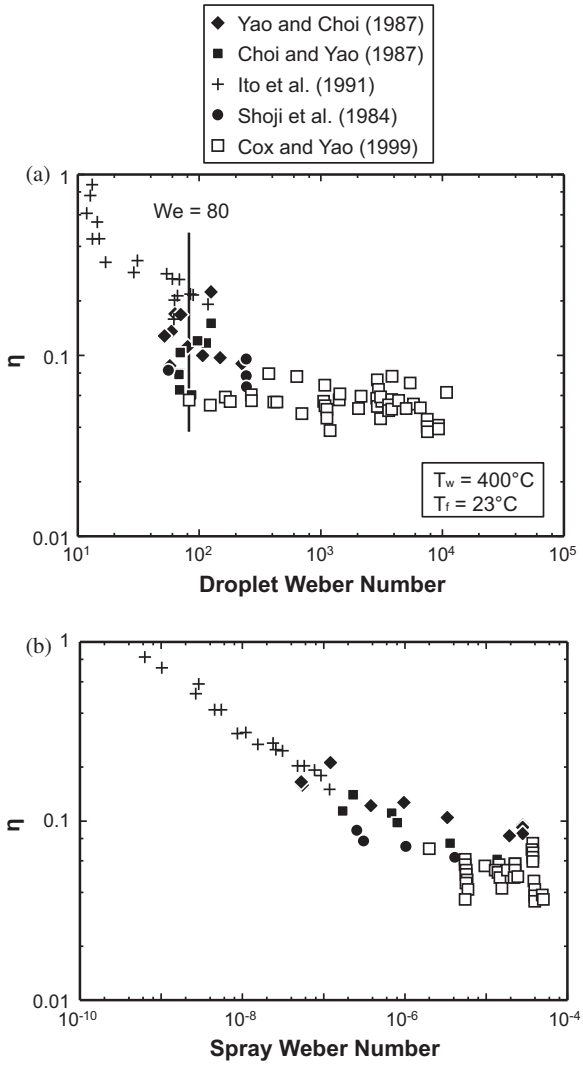

Fig. 2. Comparison of heat transfer effectiveness for water versus (a) droplet Weber number and (b) spray Weber number for $T_w = 400$ °C and $T_f = 23$ °C. Adapted from Yao and Cox [45].

momentum as they impact the liquid film covering the surface, and their temperature increases as they mix with the relatively high temperature film. Third, a new droplet impacting the surface will encounter a lower surface temperature than the previous droplet, and the time available for the surface temperature to recover decreases with increasing droplet intensity. Since the heat transfer effectiveness in the film boiling regime decreases with decreasing temperature, such consecutive impact tends to decrease effectiveness with increasing We_s. It should be noted that the data jump captured in Fig. 2(a) around $We_d = 80$ is associated with a droplet disintegration threshold following impact.

Labergue et al. [48] reported that Eq. (24) tends to underestimate their own data for water sprays. More recently, Labergue et al. [49] used a three-color laser induced fluorescence technique along with a Phase Doppler Velocimeter to demonstrate that the temperature of droplets increases with increasing incident Weber number.

4. Leidenfrost temperature

The Leidenfrost temperature, T_L, is of paramount importance to metal alloy quenching since it marks the transition from very poor heat transfer in film boiling to the far more superior heat transfer associated with transition boiling. Since faster quenching is essential to achieving superior material properties, metal manufacturers employ a variety of techniques to shift the Leidenfrost point to higher temperatures. These facts point to the importance of the ability to accurately predict and control the Leidenfrost point.

Hoogendoorn and den Hond [50] reported that models and correlations for the Leidenfrost point for a single droplet have little predictive value for sprays. They showed that T_L for water sprays varies from 350 to 900 °C, depending on spray conditions, especially volumetric flux. Experiments by Gottfried et al. [51] confirmed the strong dependence of T_L on volumetric flux. Sozbir et al. [52,53] and Al-Ahmadi and Yao [37] also reported that T_L for water sprays is influenced by local spray flux, but fairly insensitive to droplet size, droplet velocity, or nozzle type. Al-Ahmadi and Yao correlated their Leidenfrost temperature data according to

$$T_L = 536.8G^{0.116} \tag{25}$$

for $G = 1.5$–30 kg s^{-1}/m^2. Yao and Cox [45] considered the surface chilling effect resulting from heat transfer at higher mass fluxes and recommended the following correlation for high mass fluxes:

$$T_L = 1400We_s^{0.13}. \tag{26}$$

As shown in Fig. 3, Eq. (26) has been validated against data from numerous sources. Additionally, measurements by Labergue et al. [48] at high mass fluxes agree well with this correlation. Aside from the dominant influence of We_s, parameters that have a relatively lesser influence on T_L include surface roughness and thermal conductivity of the sprayed surface.

Leidenfrost temperature models for sprays are quite sparse. Bernardin and Mudawar [54] extended their sessile droplet Leidenfrost model [55] to sprays by accounting for changes in the fluid properties at the liquid-solid interface resulting from interfacial pressure rise created by the impact. This pressure rise was determined using a model by Engel [56,57] for elastic impact pressure by

$$\Delta P = 0.20\rho_f u_d u_{sound}, \tag{27}$$

where u_{sound} is the speed of sound in the liquid.

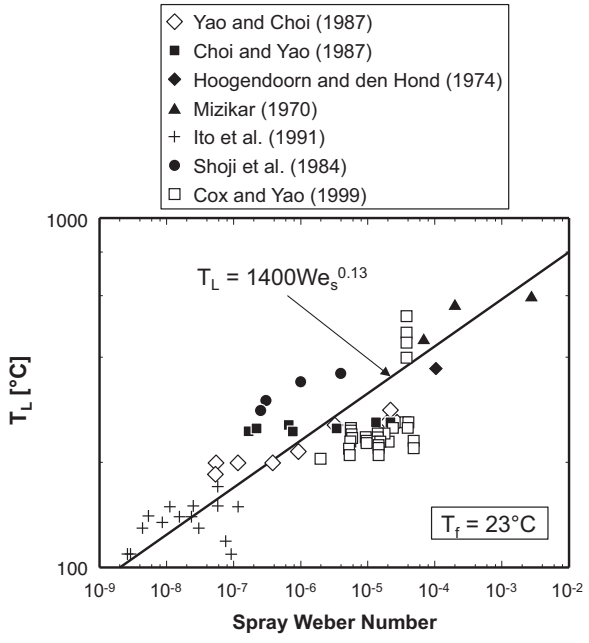

Fig. 3. Correlation of Leidenfrost temperature with spray Weber number. Adapted from Yao and Cox [45].

5. Spray quenching of metal alloy parts

5.1. Significance of heat treatment

Heat treatment plays a significant role in dictating the material properties of metal alloy parts. This process involves heating the part to a temperature slightly below melting point, followed by fast quenching to room temperature, and then reheating the part to an intermediate temperature. Given the fast temperature changes associated with the quenching phase of heat treatment, poor control of the quenching process often leads to many part imperfections, and correcting these imperfections is very costly. For example post treatment of poorly quenched aluminum extrusions accounts for nearly 50% of the production cost [11].

Presently, the vast majority of heat treatment operations involve bath quenching rather than spray quenching. This trend is driven by the low cost of bath quenching and an industry-wide lack of technical knowhow concerning the implementation and optimization of spray quenching. Yet, spray quenching is far superior to bath quenching in two major ways. First, sprays produce much faster cooling rates. Second, spray quenching offers tremendous benefits when cooling complex-shaped parts, which can be explained as follows. In bath quenching, parts of different sizes and shapes are quenched together, which causes smaller parts to cool faster than larger one, and thin sections of a complex-shaped part to cool much faster than thick sections. These limitations can trigger many imperfections in the part, including poor mechanical properties and thermally induced stresses. On the other hand, spray quenching can overcome these defects by providing mush faster cooling rates, and more uniform cooling of complex-shaped parts. The latter advantage is realized by impacting thick, high thermal mass sections of the part with dense sprays, and thin sections with light sprays, thereby allowing the part to cool both quickly and uniformly.

These advantages served as foundation for an intelligent quenching technology using water sprays that was developed in the late 1980s at the Purdue University Boiling and Two-Phase Flow Laboratory (PU-BTPFL). The first and key component of this technology consists of correlations for spray heat flux versus surface-to-fluid temperature difference for different nozzle types and operating conditions. Solving the heat diffusion equation for an initially high-temperature three-dimensional metal alloy part in response to spray cooling yields a detailed record of spatial and temporal distributions of the part's temperature. The second component of this technology is a comprehensive database for pressure spray nozzles of different patterns (*e.g.*, full cone or flat) and sizes, for which spray parameters can be determined in terms of nozzle pressure drop and water temperature. The third component is a database for metallurgical transformation kinetics for different metal alloys, which can be combined with the part's spatial and temporal distributions to predict three-dimensional distributions of key mechanical properties, such as hardness and tensile strength, as will be discussed below.

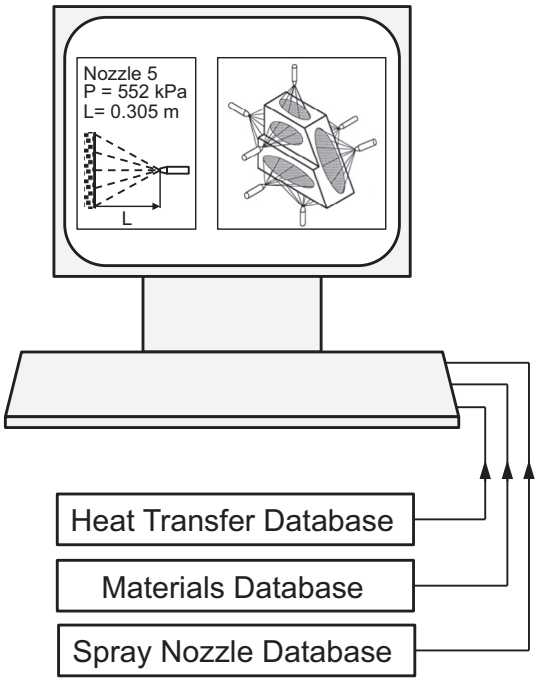

Fig. 4. CAD-based intelligent spray-quenching system.

Fig. 4 shows how the intelligent quenching technology combines information from the above three components using Computer-Aided Design (CAD) to predict the part's mechanical properties in response to the spray quench. In a production facility, the operator of the CAD system would simply input initial temperature, shape, and alloy composition of the part, and, upon consulting its extensive databases, the CAD system would determine the nozzle type, placement, and pressure drop necessary to achieving acceptable mechanical properties within the heat treated product.

5.2. Metallurgical aspects

Using an aluminum alloy as example, Fig. 5(a) shows the aluminum-rich region of the aluminum-copper phase diagram and approximate composition range (indicated by the shaded region). The heat treatment process commences by heating the alloy part to the solution heat treatment temperature, which is below the *liquidus* temperature corresponding to complete melting of the alloy [58]. More specifically, the solution heat treatment temperature is above the *solvus* temperature (point where copper becomes soluble within aluminum), but below the *solidus* temperature (point where the alloy begins to melt). When maintained above the solvus temperature for a sufficient time, the copper (solute) diffuses completely into the aluminum (solvent) to form a solid solution. Subsequent cooling – quenching – below the solvus temperature results in a supersaturated solid solution that seeks equilibrium by precipitating the hardening solute, $CuAl_2$. As shown in Fig. 5(a), different microstructures will result when the part is cooled to near room temperature, depending on cooling rate. Very rapid cooling preserves the initial homogeneous supersaturated solid solution, and results in an alloy that is age-hardenable during the subsequent aging process, the third and final stage of heat treating. Conversely, very slow cooling causes coarse $CuAl_2$ precipitates to form along the grain boundaries, resulting in an alloy that cannot be age-hardened.

As shown in Fig. 5(b), aging is achieved by heating the alloy to an intermediate temperature (between preheat and room temperatures) over an appropriate duration to promote *fine dispersion* of precipitates within the aluminum grains, which serve as dislocation barriers and impart the desired increases in strength and hardness. However, over-aging can cause further coalescence into a more *coarse dispersion*, reducing the number of dislocation barriers, thus compromising both strength and hardness.

It is obviously highly desirable to cool the entire alloy part as fast as possible from the solution heat treatment temperature as shown in Fig. 5(a). However, this is not possible for large parts. Additionally, rapid quenching of the exterior of a part having a cross section with large thickness variations causes the interior of thin sections to cool much quicker than the interior of thick sections. This would lead to high thermal stresses caused by large spatial temperature gradients during the quench, along with residual stresses and possible warping, as shown in Fig. 6. On the other

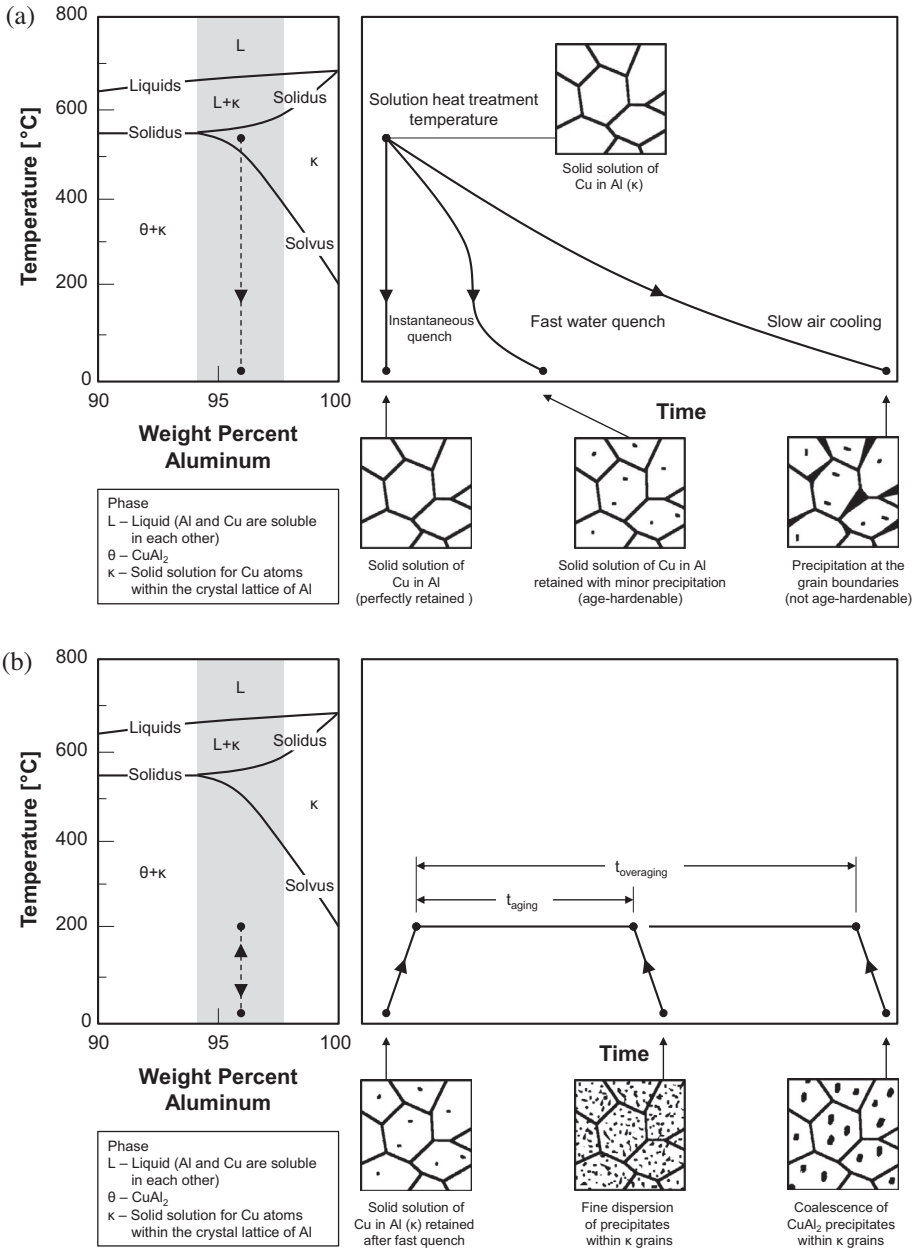

Fig. 5. Aluminum-rich region of Al-Cu phase diagram and microstructure that develops following (a) quenching and (b) subsequent aging of an Al-Cu (4.4 wt%) alloy. Adapted from Hall and Mudawar [58].

hand, slow cooling ensures spatial uniformity of the part's temperature, but precludes the ability to achieve the desired strength or hardness during the aging process because of the massive precipitation of solutes along the aluminum grain boundaries [59]. Consequently, an optimum cooling strategy exists within a window of acceptable cooling rates such that the part is cooled as quickly and uniformly as possible. This is achieved by proper placement and operation of the spray nozzles, where the local heat flux everywhere along the surface is controlled such that all locations in the part's interior are optimally cooled.

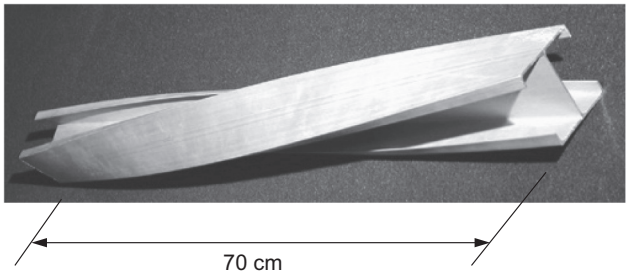

Fig. 6. Warping and distortion of an initially two-dimensional aluminum alloy extrusion having an H-shaped cross section due to poorly configured spray quenching.

5.3. Consolidated heat transfer correlations for water spray quenching

The intelligent quenching technology was proposed initially by Deiters and Mudawar [60] in 1989 to optimize the process of spray quenching following extrusion, forging, or continuous casting. They also described a numerical scheme to demonstrate how controlled spray quenching of products containing sections of differing thicknesses can significantly reduce thermal gradients. They solved the heat diffusion equation for an aluminum alloy part using local

correlations by Mudawar and Valentine [11] for spray heat flux versus surface-to-fluid temperature difference. These correlations were based on droplet diameter, droplet velocity, and local volumetric flux, which were all measured independently. The correlations included detailed relations for the single-phase, nucleate boiling, and transition boiling regimes for surface temperatures below 400 °C, but not the film boiling regime. Deiters and Mudawar [61,62] employed these correlations as boundary conditions in a three-dimensional heat diffusion model of a rectangular aluminum block quenched along one surface by a spatially varying water spray. They showed that the correlations of Mudawar and Valentine are both spatially universal and applicable to all types of sprays (full cone, hollow cone, and flat) employed in materials processing.

Later, Klinzing et al. [13] derived complementary correlations for both the transition and film boiling regimes for low volumetric flux ($Q'' < 3.5 \times 10^{-3}$ m^3 s^{-1}/m^2) and high volumetric flux ($Q'' > 3.5 \times 10^{-3}$ m^3 s^{-1}/m^2) sprays. Using these correlations along with Mudawar and Valentine's correlations for the single-phase and nucleate boiling regimes, they successfully predicted the temperature response of a rectangular aluminum alloy plate. Rozzi et al. [63] described the construction of a large-scale spray quenching test bed to mimic industrial spray quenching of complex-shaped aluminum alloy parts. They measured the temperature response of an L-shaped aluminum alloy part to spray cooling, which they accurately predicted using the same methodology adopted by Klinzing et al.

One difficulty in using the correlations developed by Mudawar and Valentine and Klinzing et al. is associated with discontinuities at the point of departure from film boiling (DFB) and the Leidenfrost point or minimum heat flux (MIN). Hall and Mudawar [59] revised the earlier correlations for the high temperature boiling regimes in an effort to produce a smooth and continuous boiling curve for different combinations of the spray hydrodynamic parameters. This was accomplished by matching both heat flux and heat flux slope along the boiling curve. At DFB, (*i.e.*, $\Delta T_f = \Delta T_{DFB}$) they set

$$q'' = q''_{DFB}, \tag{28a}$$

and

$$\frac{\partial q''}{\partial \Delta T_f} = \left.\frac{\partial q''_{FB}}{\partial \Delta T_f}\right|_{DFB}, \tag{28b}$$

and at MIN (*i.e.*, $\Delta T_f = \Delta T_{MIN}$),

$$q'' = q''_{MIN}, \tag{29a}$$

and

$$\frac{\partial q''}{\partial \Delta T_f} = \left.\frac{\partial q''_{TB}}{\partial \Delta T_f}\right|_{MIN} = 0. \tag{29b}$$

Reformulating the correlation for DFB temperature poses the possibility of a DFB temperature lower than the MIN temperature or a boiling curve with a steeper slope in the film wetting regime than in the film boiling regime; both of which are encountered with relatively low volumetric fluxes, which implies the absence of the film wetting regime.

Table 2 provides a consolidated summary of spray quenching correlations by Mudawar and Valentine [11], Klinzing et al. [13], Rybicki and Mudawar [64], and Estes and Mudawar [65], including the slope corrections by Hall and Mudawar [59].

5.4. Quench factor technique

The quench factor technique couples the time required for precipitation of hardening solute, in the form of the *C-curve* (described below), with the time available for precipitation, represented by the temperature-time curve of the quenched part. This technique employs a parameter termed quench factor, τ, which can be used to assess the influence of quench rate on ultimate strength and hardness of the metal alloy part. It is defined as

$$\tau = \int_{t_i}^{t_f} \frac{dt}{C_t}, \tag{30}$$

where times t_i and t_f correspond, respectively, to the start and end of the quench, and C_t is the critical time required at different temperatures to precipitate a sufficient amount of solute to reduce the maximum attainable strength or hardness by a specific percentage (typically 99.5%), and is defined as

$$C_t = -k_1 k_2 \exp\left(\frac{k_3 k_4^2}{RT(k_4 - T)^2}\right) \exp\left(\frac{k_5}{RT}\right), \tag{31}$$

where k is an empirical constant and R the universal gas constant. Zero and infinity values of the quench factor correspond to suppression of precipitation and complete precipitation, respectively. As depicted in Fig. 7, the integral in Eq. (30) can be numerically calculated by discretizing the temperature-time cooling curve into small time increments. On the right side in Fig. 7 is the corresponding relation between C_t and temperature, the *C-curve*. An incremental quench factor associated with each time increment represents the ratio of the amount of time the alloy is at a specific temperature to the amount of time required to obtain a specified amount of transformation at the same temperature. Overall, the non-isothermal quench can be treated as a series of isothermal quenches, which are additive if the alloy obeys the rule of additivity over the entire range of transformation temperatures, and the quench factor can be approximated as

$$\tau = \sum_{m=1}^{n} \frac{\Delta t_m}{C_{t,m}}. \tag{32}$$

Overall, the importance of the magnitude of τ is exemplified in its impact on mechanical properties, according to

$$\frac{H - H_{\min}}{H_{\max} - H_{\min}} = \frac{\sigma - \sigma_{\min}}{\sigma_{\max} - \sigma_{\min}} = \exp(k_1 \tau), \tag{33}$$

where $\sigma_{\max}$ (or $H_{\max}$) and $\sigma_{\min}$ (or $H_{\min}$) are the maximum and minimum yield strength (or hardness) of alloy specimens that are cooled at near infinite rate and extremely slow rate, respectively. Note that the coefficient k_1 in Eq. (33) is negative, which implies that superior properties are achieved by minimizing τ.

Hall and Mudawar [66] developed a method for minimizing the quench factor by taking the derivative of the quench factor with respect to temperature,

$$\frac{d\tau}{dT} = \frac{1}{C_t(dT/dt)}, \tag{34}$$

suggesting that the quench factor can be minimized by maximizing $C_t\ dT/dt$, the product of critical time and cooling rate during the quench. As shown in the C-curve in Fig. 7, the critical time at relatively high and low temperatures is extremely large, hence the cooling rate has little influence on metallurgical structure. While at intermediate temperatures, the critical time is small and cooling rate has substantial influence on the metallurgical structure. Therefore, it is at these intermediate temperatures where cooling rate, *i.e.*, dT/dt, must be maximized.

Achieving high values for dT/dt within the intermediate temperatures associated with the nose of the C-curve is closely associated with the prevalent spray regime in the same temperature range. Should film boiling be prevalent in this range, faster cooling rate can be achieved by increasing volumetric flux in order to improve

Table 2
Summary of heat transfer correlations for spray quenching.

Heat transfer regime	Correlations
Film boiling [13]	$Q'' > 3.5 \times 10\ \mathrm{m^3\ s^{-1}/m^2}$ $q''_{FB} = 1.413 \times 10^5 \Delta T_f^{0.461} Q''^{0.566} u_m^{0.639}$
	$Q'' < 3.5 \times 10\ \mathrm{m^3\ s^{-1}/m^2}$ $q''_{FB} = 63.25 \Delta T_f^{1.691} Q''^{0.264} d_{32}^{-0.062}$
DFB [59]	$q''_{DFB} = q''_{FB}\big\vert_{DFB} = 6.100 \times 10^6 Q''^{0.589} u_m^{0.244}$
	$\Delta T_{DFB} = 8.862 \times 10^2 Q''^{0.192} u_m^{0.144} d_{32}^{0.0367}$
Film-wetting [59]	If $\Delta T_{DFB} \leqslant \Delta T_{MIN}$ or $q''_{MIN} \leqslant q''_{FB}\vert_{MIN}$, then film wetting regime does not exist
	$q''_{FW} = q''_{MIN} + \frac{q''_{DFB} - q''_{MIN}}{(\Delta T_{DFB} - \Delta T_{MIN})^3} \left[(3\Delta T_{DFB} - \Delta T_{MIN}) \Delta T_{MIN}^2 - 6\Delta T_{DFB} \Delta T_{MIN} \Delta T_f \right.$
	$\left. + 3(\Delta T_{DFB} + \Delta T_{MIN}) \Delta T_f^2 - 2\Delta T_f^3 \right]$
	$+ \frac{\partial q''}{\partial \Delta T_f}\big\vert_{DFB} \frac{1}{(\Delta T_{DFB} - \Delta T_{MIN})^2} \left[-\Delta T_{DFB} \Delta T_{MIN}^2 + (2\Delta T_{DFB} + \Delta T_{MIN}) \Delta T_{MIN} \Delta T_f \right.$
	$\left. - (\Delta T_{DFB} + 2\Delta T_{MIN}) \Delta T_f^2 + \Delta T_f^3 \right]$
	$\frac{\partial q''}{\partial \Delta T_f}\big\vert_{DFB} = \frac{\partial q''_{FB}}{\partial \Delta T_f}\big\vert_{DFB} = 1.164 \times 10^4 Q''^{0.397} u_m^{0.0995} d_{32}^{-0.0366}$
Leidenfrost point [13]	$q''_{MIN} = 3.324 \times 10^6 Q''^{0.544} u_m^{0.324}$
	$\Delta T_{MIN} = 2.049 \times 10^2 Q''^{0.066} u_m^{0.138} d_{32}^{-0.035}$
	If film wetting regime does not exist, then
	$q''_{MIN} = q''_{FB}\vert_{MIN} = 5.127 \times 10^5 Q''^{0.376} u_m^{0.233} d_{32}^{-0.121}$
Transition boiling [13]	$q''_{TB} = q''_{CHF} - \frac{q''_{CHF} - q''_{MIN}}{(\Delta T_{CHF} - \Delta T_{MIN})^3} \left[\Delta T_{CHF}^3 - 3\Delta T_{CHF}^2 \Delta T_{MIN} \right.$
	$\left. + 6\Delta T_{CHF} \Delta T_{MIN} \Delta T_f - 3(\Delta T_{CHF} + \Delta T_{MIN}) \Delta T_f^2 + 2\Delta T_f^3 \right]$
CHF [11,65]	$\frac{q''_{CHF,p}}{\rho_g h_{fg} Q''} = 2.3 \left(\frac{\rho_f}{\rho_g} \right)^{0.3} \left(\frac{\rho_f Q''^2 d_{32}}{\sigma} \right)^{-0.35} \left[1 + 0.0019 \left(\frac{\rho_f c_{p,f} \Delta T_{sub}}{\rho_g h_{fg}} \right) \right]$
	$\Delta T_{CHF} = 18 \left[\rho_g h_{fg} Q'' \left(\frac{\sigma}{\rho_f Q''^2 d_{32}} \right)^{0.198} \right]^{1/5.55}$
Nucleate boiling [64]	$\frac{q''_{NB} d_{32}}{\mu_f h_{fg}} = 4.79 \times 10^{-3} \left(\frac{\rho_f}{\rho_g} \right)^{2.5} \left(\frac{\rho_f \overline{Q}''^2 d_{32}}{\sigma} \right)^{0.35} \left(\frac{c_{p,f} \Delta T_f}{h_{fg}} \right)^{5.75}$
Incipient boiling [11]	$\Delta T_f = 13.43 Re_s^{0.167} \mathrm{Pr}_f^{0.123} \left(\frac{k_f}{d_{32}} \right)^{0.220}$
Single-phase cooling [64]	$Nu = 4.70 Re_s^{0.61} \mathrm{Pr}_f^{0.32}$

Note: Units of parameters are q'' [W/m^2], $\Delta T_f = T_w - T_f$ [°C], Q'' [m^3 s^{-1}/m^2], u_m [m/s], d_{32} [m], ρ [kg/m^3], h_{fg} [J/kg], $c_{p,f}$ [J/kgK], k_f [W/mK], μ_f [Ns/m^2], σ [N/m]. $(T_w + T_f)/2$ is used in single-phase regime and saturation temperature in the other regimes to evaluate fluid properties.

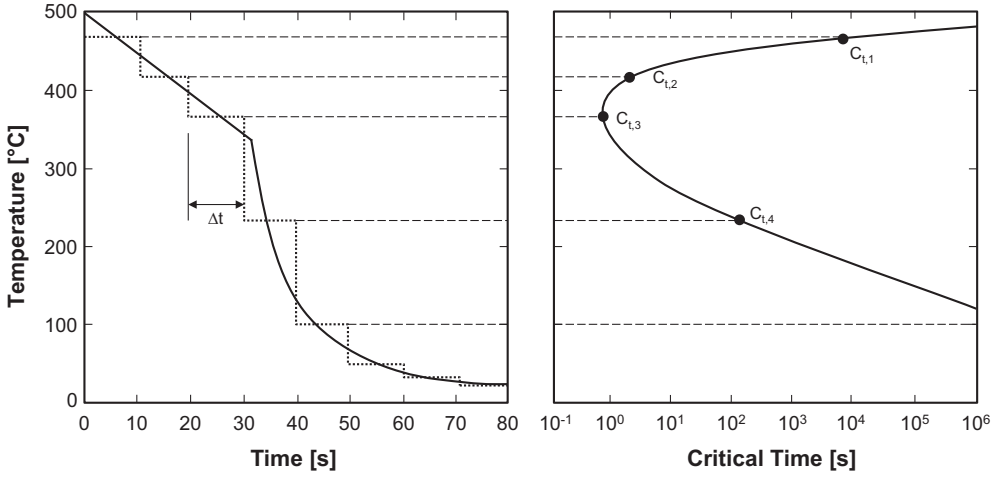

Fig. 7. Numerical calculation of quench factor using the temperature-time curve and C-curve. Adapted from Hall and Mudawar [58].

film boiling heat transfer. This can be accomplished by increasing the nozzle's pressure drop or opting for a higher capacity nozzle. Another effective strategy is to switch from film boiling to transition boiling at a higher Leidenfrost temperature, in order to take advantage of the faster cooling rate associated with transition boiling.

5.5. Optimization and validation

Typically, a quenching operation consists of either stationary parts or long extrusions moving through an array of spray nozzles. When quenching a long part with uniform two-dimensional cross-section, even spray coverage can be achieved by utilizing several nozzles with overlapping spray impact areas. However, it is crucial that the nozzle spacing should be optimized to avoid axial variations in the heat transfer coefficient. Overall, volumetric spray flux is the primary spray hydrodynamic parameter controlling the spatial variation of the heat transfer rate since d_{32} and u_m are relatively insensitive to location for pressure sprays [61]. Hall and Mudawar [67] developed an additive methodology, where the volumetric flux distributions for two side-by-side nozzles are superimposed, and an optimum distance between the nozzles is selected to ensure

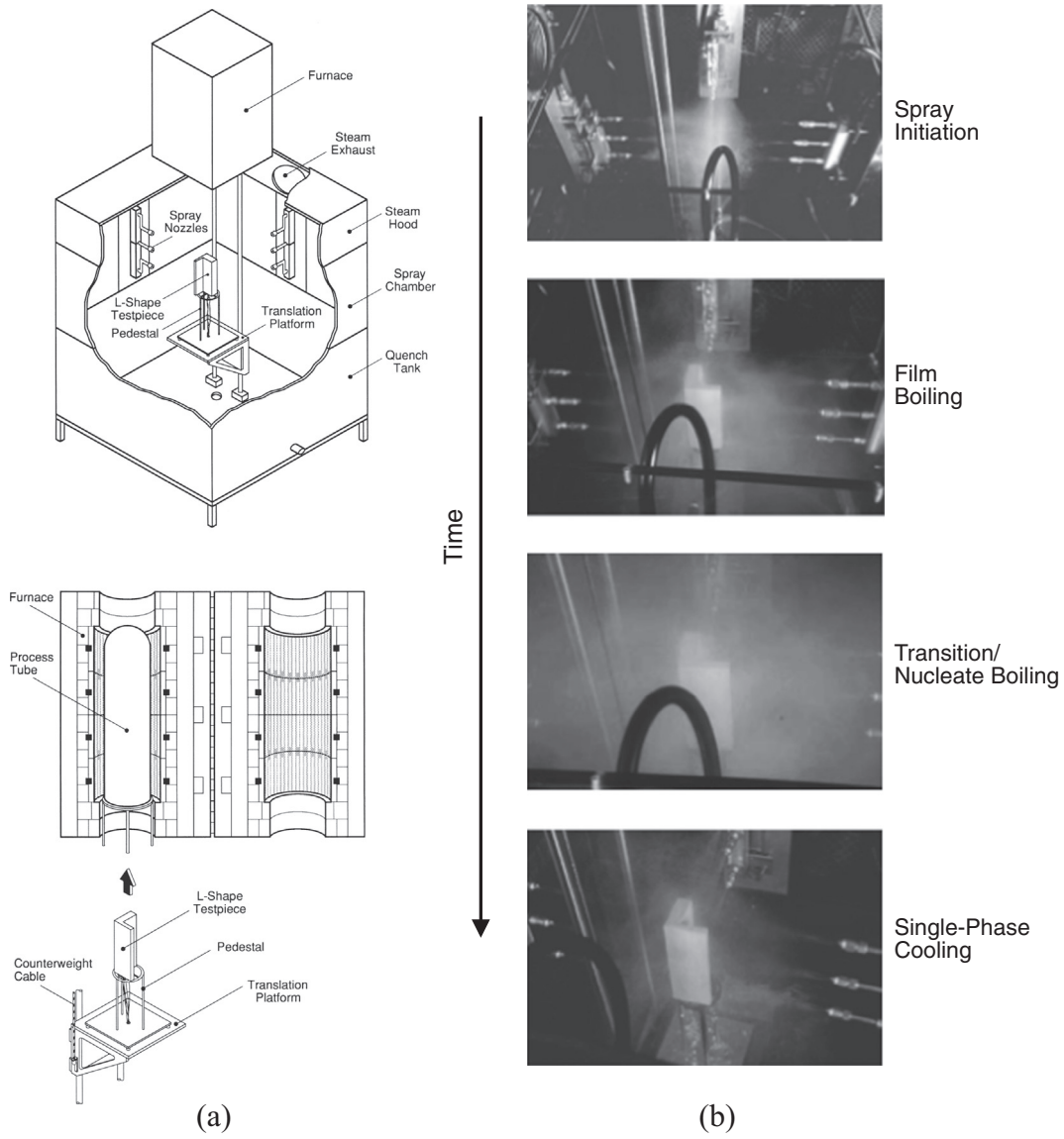

Fig. 8. (a) Schematic diagram of spray quenching test bed and platform used to translate alloy part from the furnace atop down into the spray chamber (adapted from Hall and Mudawar [58]). (b) Images of spray quenching of two-dimensional L-shaped aluminum alloy part. Four arrays of nozzles, each containing three nozzles, are strategically configured to impact four vertical surfaces of the part at optimized flow conditions.

axially uniform volumetric flux and, hence, preclude axial variations in the spray heat transfer coefficient.

Hall and Mudawar [67] examined the quenching of an L-shaped aluminum alloy part, with one section several times thicker than the other, in the spray test bed depicted in Fig. 8(a). They measured the cooling history at different locations within the part, and later measured the hardness at the same locations. Fig. 8(b) shows images of the L-shape quenching, with the sprays initiated before the part is lowered into the spray chamber. Once the pre-heated part enters the spray chamber, film boiling is established along all its surfaces, followed by transition boiling, nucleate boiling, and eventually single-phase cooling. Notice the limited vapor production in the spray chamber within the film boiling regime since the vapor is mostly trapped close to the part surfaces. Intense vapor product ensues in both the transition boiling and nucleate boiling regimes, but eventually subsides in the single-phase regime. Using the consolidated heat transfer correlations provided in Table 2, they solved the heat diffusion equation for the part and demonstrated close predictions of the measured cooling history for different spray boundary conditions. They then used the quench factor technique to calculate the distribution of hardness within the part, and showed excellent agreement with the measured hardness values [58]. Fig. 9 shows excellent agreement between measured and predicted hardness distributions for the L-shaped part when purposely cooled along one surface of the thin section to induce appreciable hardness gradients. Hall and Mudawar [66] also showed optimal selections of spray nozzle and nozzle pressure drop for individual surfaces of the quenched part, with which it is possible to simultaneously achieve all crucial goals of the heat treatment: (1) fast cooling, in pursuit of superior mechanical properties, and (2) uniform temperature everywhere within the part, to preclude warping caused by thermal and residual stresses.

Bernardin and Mudawar [68] experimentally examined the influence of surface roughness on spray quenching with the aid of scanning electron microscopy, surface contact profilometry, and X-ray photoelectron spectroscopy. They employed aluminum

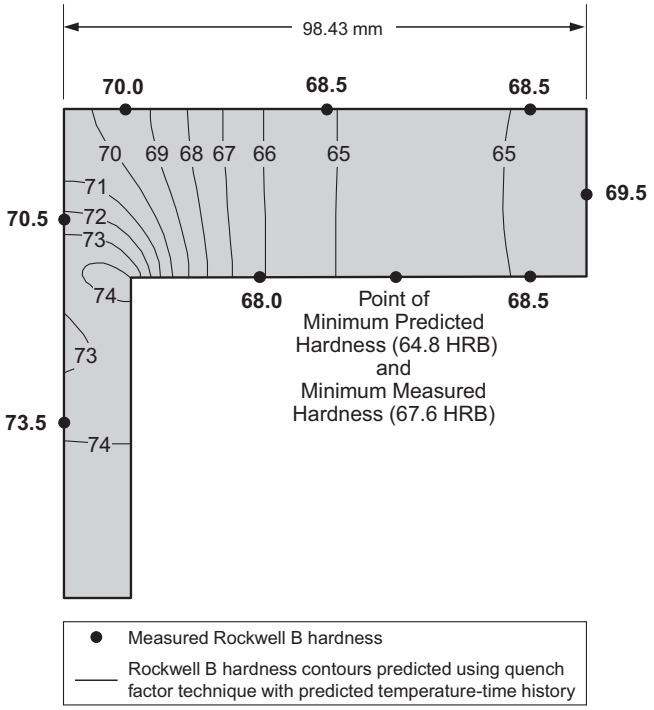

Fig. 9. Measured Rockwell B hardness of the heat treated L-shape and hardness predicted using the quench factor technique and predicted temperature-time history. Adapted from Hall and Mudawar [58].

samples with a variety of initial surface roughnesses, that were subjected to repeated heat-quench cycles, and observed measurable changes in surface roughness, whose magnitude was dependent upon the initial surface finish and alloy composition. These changes included both small scale roughness features (up to 25 μm), which influenced cooling rate by increasing the number of bubble nucleation sites during transition and nucleate boiling, and, more importantly, large blisters (25–1000 μm) that influenced droplet impact and spread, as well as the Leidenfrost temperature. Bernardin and Mudawar [69] also noted that repeated heat-quench cycles tend to shift the temperature-time cooling curve towards shorter overall quench periods.

5.6. Quenching of cylindrical surfaces

In the past, quenching of cylindrical surfaces was achieved using air-assist water sprays [70–73]. However, given the large spatial variations in volumetric flux within the spray impact area, and therefore non-uniformity in surface heat flux, better and more predictable performance may be realized with pressure sprays. Recently, Mascarenhas and Mudawar [3] examined the quenching of a solid alloy cylinder using water sprays produced by full cone pressure nozzles. Shown in Fig. 10(a) is a schematic diagram of the quenching system, consisting of a solid metal alloy cylinder that is subjected to an array of identical pressure sprays. Maximum surface exposure to the liquid was achieved by arranging the sprays circumferentially as well as longitudinally such that their impact areas on the cylindrical surface were tangent to one another. Another advantage of this configuration is the ease of determining spray nozzle layout in a heat-treating plant. Fig. 10(b) shows a representative unit cell of the system, consisting of a sector of the cylinder subjected to a single spray. A key difficulty in assessing the cooling performance of the sprays is the spatial distribution of volumetric flux resulting from the surface curvature. Using the spray model illustrated in Fig. 11, Mascarenhas and Mudawar derived an analytical model to determine the distribution of volumetric flux across the *convex surface* of the cylinder,

$$\frac{Q''}{\overline{Q}''} = \left[\frac{\tan(\theta/2)\sin\varphi}{1-\cos(\theta/2)}\right]\left[1+(r/H)^2\right]^{-3/2} \times \left[\frac{\sin\beta}{(r/H)} - \frac{\cos\beta}{1+(r/H)^2} + \frac{1}{1+(r/H)^2}\left(\frac{2H}{D}+1\right)\frac{1}{1-(r/H)\tan\beta}\right]^{-1}, \tag{35}$$

where

$$\overline{Q}'' = \frac{Q}{\pi[H\tan(\theta/2)](D\sin\varphi/2)}, \tag{36a}$$

$$\varphi = \sin^{-1}\left[\left(\frac{2H}{D}+1\right)\sin(\theta/2)\right] - \theta/2, \tag{36b}$$

and

$$\beta = \sin^{-1}\left[\left(\frac{2H}{D}+1\right)\frac{(r/H)}{\sqrt{1+(r/H)^2}}\right] - \tan^{-1}(r/H). \tag{36c}$$

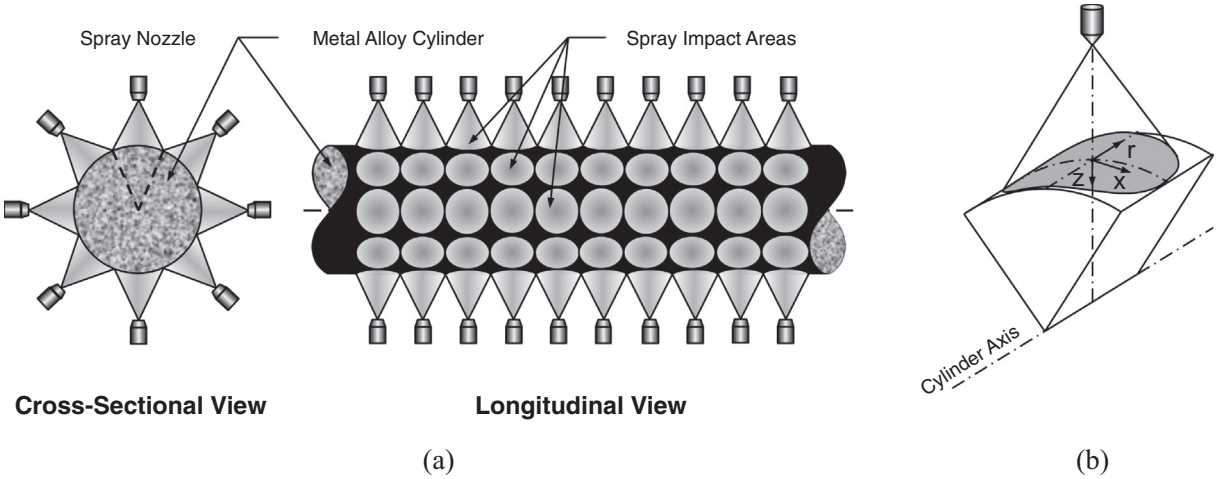

Fig. 10. (a) Spray nozzle configuration for quenching of solid metal alloy cylinder, and (b) unit quenching cell. Adapted from Mascarenhas and Mudawar [3].

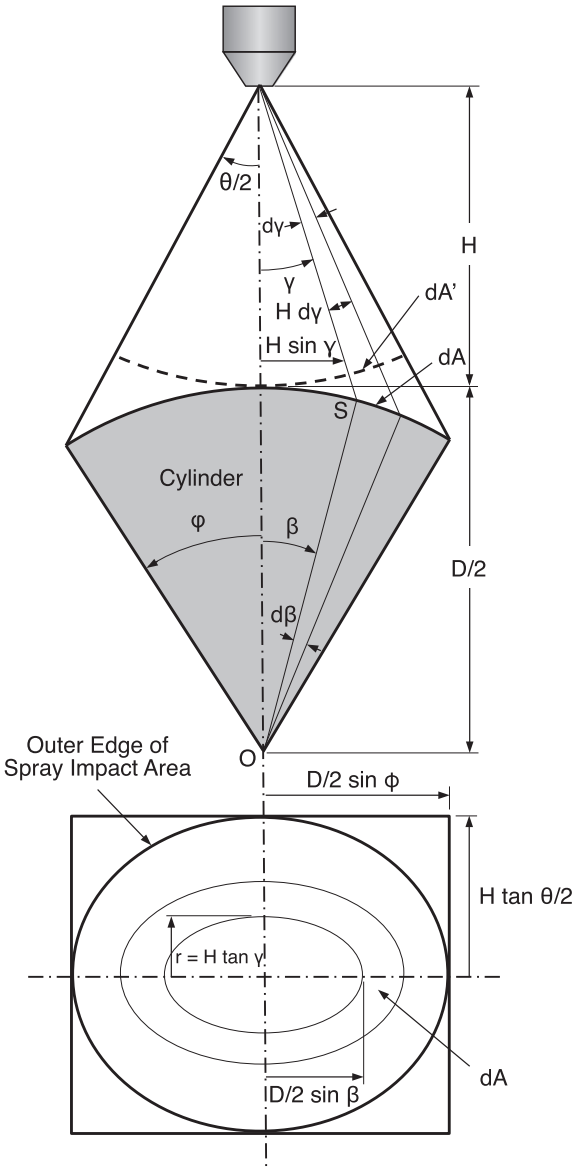

Fig. 11. Spray model for unit cell of convex cylindrical surface. Adapted from Mascarenhas and Mudawar [3].

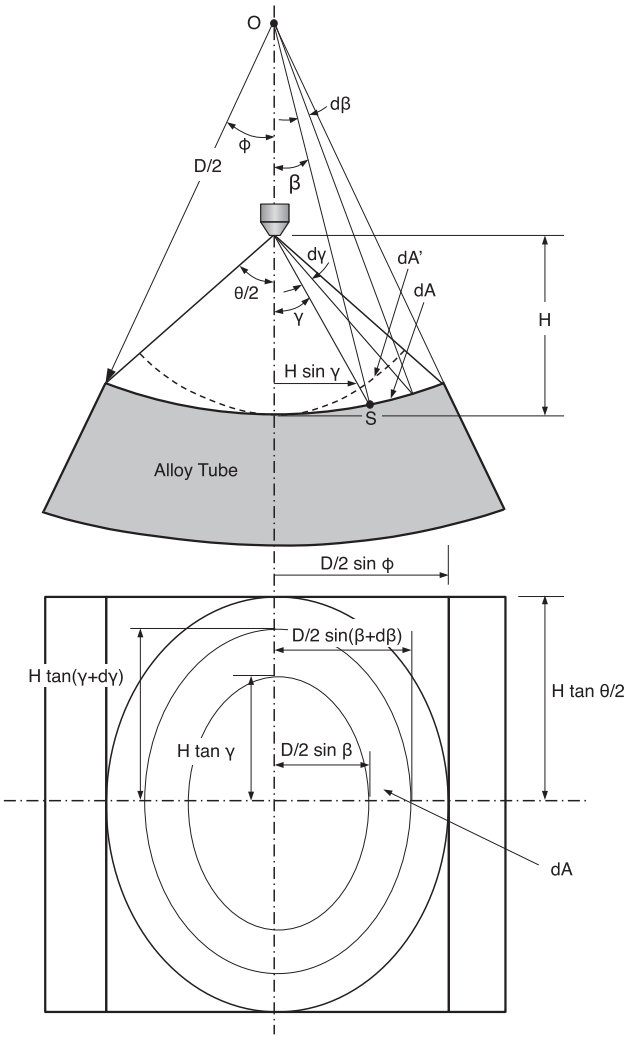

Fig. 13. Spray model for unit cell of concave cylindrical surface. Adapted from Mascarenhas and Mudawar [74].

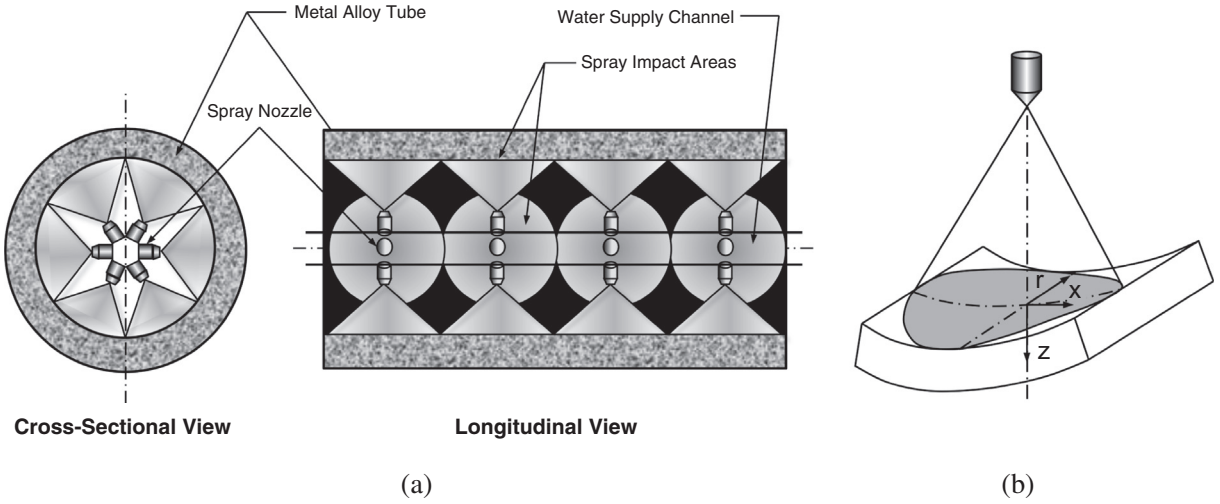

Fig. 12. (a) Spray nozzle configuration for quenching of metal alloy thick-walled tube, and (b) unit cell. Adapted from Mascarenhas and Mudawar [74].

This distribution was combined with the spray heat transfer correlations provided in Table 2 for all boiling regimes and transition points to generate a local boiling curve for every location on the impact surface. Using these boiling curves as boundary conditions, the transient three-dimensional heat diffusion equation was solved for aluminum alloy and steel cylinders subject to different values of spray nozzle pressure drop and nozzle-to-surface distance.

Later, Mascarenhas and Mudawar [74] extended this methodology to internal spray quenching of thick-walled metal alloy tubes. Fig. 12(a) and (b) show the corresponding nozzle configuration and unit quenching cell, respectively. And, utilizing the geometrical spray model shown in Fig. 13, they derived the spatial distribution of volumetric flux for the inner *concave surface* of the tube,

$$\frac{Q''}{\overline{Q''}} = \left[\frac{\tan(\theta/2)\sin\varphi}{1-\cos(\theta/2)}\right]\left[1+(r/H)^2\right]^{-3/2} \times \left[\frac{\sin\beta}{(r/H)} - \frac{\cos\beta}{1+(r/H)^2} + \frac{1}{1+(r/H)^2}\left(\frac{2H}{D}-1\right)\frac{1}{1+(r/H)\tan\beta}\right]^{-1}, \tag{37}$$

where

$$\varphi = \sin^{-1}\left[\left(\frac{2H}{D}-1\right)\sin(\theta/2)\right] + \theta/2 \tag{38a}$$

and

$$\beta = \sin^{-1}\left[\left(\frac{2H}{D}-1\right)\frac{(r/H)}{\sqrt{1+(r/H)^2}}\right] + \tan^{-1}(r/H). \tag{38b}$$

By setting boundary conditions for both the sprayed and unsprayed portions of the tube surface, a transient heat diffusion model was constructed for the unit cell for both aluminum alloy and steel tubes. The model yielded quench curves for all points along the sprayed surface and within the tube wall. This approach also facilitates the determination of surface temperature gradients in the quenched part to guard against stress concentration. Fig. 14 compares spray quench curves for aluminum alloy and steel tubes that are sprayed only along the inner surface. Notice the appreciable differences in thermal response between the two alloys. The inner sprayed surface is shown to cool much faster for steel than for aluminum. On the other hand, the outer unsprayed surface cools a lot slower in steel than in aluminum. These trends are closely related to the large difference in thermal diffusivities between the two alloys, 1.25×10^{-5} m^2/s for steel compared to 8.07×10^{-5} m^2/s for aluminum. With its highly superior thermal diffusivity, aluminum promotes faster penetration of the cooling effect through the tube wall, rapidly dissipating the surface temperature gradient and reducing cooling rate along the sprayed surface, and decreasing temperatures within the tube wall. Steel, on the other hand, is far slower in conducting the heat away from the surface and into the tube wall.

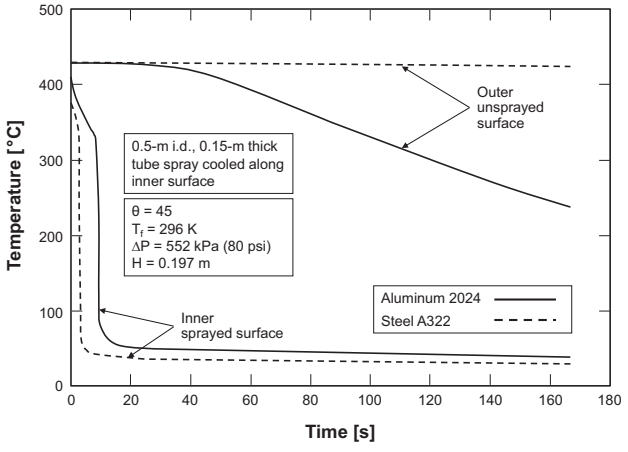

Fig. 14. Comparison of spray quench curves for aluminum and steel tubes. Adapted from Mascarenhas and Mudawar [74].

The above findings demonstrate the effectiveness of combining (a) the universal water spray correlations, (a) the volumetric flux models for flat, convex, and concave surfaces, and (c) the quench factor technique to both predict and optimize the quenching of complex-shaped metal alloy parts in pursuit of both fast and uniform cooling, and superior mechanical properties.

6. Concluding remarks

This paper is the second part of a two-part review of spray cooling. The first part addressed the single-phase and nucleate boiling regimes, as well as critical heat flux (CHF), which are important to cooling relatively lower temperature high-heat-flux devices. The present part addresses the complementary higher temperature transition boiling and film boiling regimes, as well as the Leidenfrost point. Also discussed is how spray heat transfer correlations and models can be implemented as boundary conditions in heat diffusion models of metal alloy parts to accurately predict the temperature-time (quench) history everywhere within the part. Key observations from this review can be summarized as follows.

(1) Published studies on spray film boiling and, especially, transition boiling are quite limited in terms of identifying dominant mechanisms and recommending predictive correlations and/or more models. Clearly, future studies addressing these two regimes must be conducted with more sophisticated instrumentation and imaging methods to more accurately capture near-surface droplet impact, liquid film behavior, and vapor film formation for many liquids with drastically different thermophysical properties, and over broad ranges of operating conditions.

(2) The spray Leidenfrost point plays a crucial role in metal part quenching since its marks the transition between slow film boiling and much faster transition boiling as the part is quenched from high temperature. However, published works addressing the Leidenfrost point have been focused mostly on single droplets, while those concerning sprays are quite sparse. More attention must therefore be focused in future studies on dominant mechanisms as well as predictive tools specific to the Leidenfrost point in sprays.

(3) Correlations for the different spray boiling regimes and transition points are paramount to the prediction of temperature-time cooling curve for metal alloy parts during quenching. Combining the quench curve with metallurgical transformation kinetics provides an accurate and robust means for predicting the strength and hardness of metal alloy parts. By strategically configuring the spray system used to quench complex-shaped parts, it is also possible to greatly enhance these mechanical properties while avoiding high residual stresses. This approach requires accurate models of volumetric flux distribution for flat, concave and convex surfaces of the quenched part.

Conflict of Interest

Authors stat that there is no conflict of interest.

Acknowledgements

Support of the National Natural Science Foundation of China under Grant No. 51506023, the China Postdoctoral Science Foundation under Grant No. 2016T90220, and the Fundamental Research Funds for Central Universities of Ministry of Education of China are gratefully acknowledged.

References

[1] G. Liang, I. Mudawar, Review of spray cooling-Part 1: Single-phase and nucleate boiling regimes, and critical heat flux, Int. J. Heat Mass Transfer 115 (2017) 1174–1205.
[2] I. Mudawar, Recent advances in high-flux, two-phase thermal management, J. Therm. Sci. Eng. Appl. Trans. ASME 5 (2013) 021012.
[3] N. Mascarenhas, I. Mudawar, Analytical and computational methodology for modeling spray quenching of solid alloy cylinders, Int. J. Heat Mass Transfer 53 (2010) 5871–5883.
[4] R. Wendelstorf, K.-H. Spitzer, J. Wendelstorf, Effect of oxide layers on spray water cooling heat transfer at high surface temperatures, Int. J. Heat Mass Transfer 51 (2008) 4892–4901.
[5] S. Toda, A study of mist cooling (1st Report: Investigation of mist cooling), Heat Transfer-Jap. Res. 1 (1972) 39–50.
[6] M. Monde, Critical heat flux in the saturated forced convection boiling on a heated disk with impinging droplets, Trans. JSME 45 (1980) 849–858.
[7] M.R. Pais, D.E. Tilton, L.C. Chow, E.T. Mahefkey, High-heat-flux, low-superheat evaporative spray cooling, in: 27th AIAA Aerospace Sciences Meeting, AIAA, Reno, USA, Springer, Reno, USA, 1989.
[8] K.J. Choi, S.C. Yao, Mechanisms of film boiling heat transfer of normally impacting spray, Int. J. Heat Mass Transfer 30 (1987) 311–318.
[9] Q. Cui, S. Chandra, S. McCahan, The effect of dissolving salts in water sprays used for quenching a hot surface: Part 2-Spray cooling, J. Heat Transfer – Trans. ASME 125 (2003) 333–338.
[10] Y.M. Qiao, S. Chandra, Spray cooling enhancement by addition of a surfactant, J. Heat Transfer – Trans. ASME 120 (1998) 92–98.
[11] I. Mudawar, W.S. Valentine, Determination of the local quench curve for spray-cooled metallic surfaces, J. Heat. Treat. 7 (1989) 107–121.
[12] R. Dou, Z. Wen, G. Zhou, Heat transfer characteristics of water spray impinging on high temperature stainless steel plate with finite thickness, Int. J. Heat Mass Transfer 90 (2015) 376–387.
[13] W.P. Klinzing, J.C. Rozzi, I. Mudawar, Film and transition boiling correlations for quenching of hot surfaces with water sprays, J. Heat. Treat. 9 (1992) 91–103.
[14] J.D. Bernardin, I. Mudawar, Transition boiling heat transfer of droplet streams and sprays, J. Heat Transfer 129 (2007) 1605–1610.
[15] G.W. Liu, Y.S. Morsi, B.R. Clayton, Characterisation of the spray cooling heat transfer involved in a high pressure die casting process, Int. J. Therm. Sci. 39 (2000) 582–591.
[16] J.K. Brimacombe, P.K. Agarwal, L.A. Baptista, S. Hibbins, B. Prabhakar, Spray cooling in the continuous casting of steel, in: Proc. 63rd National Open Hearth and Basic Oxygen Steel Conference, Washington D.C., USA, 1980, pp. 235–252.
[17] L. Bolle, J.C. Moureau, Spray cooling of hot surfaces: a description of the dispersed phase and a parametric study of heat transfer results, in: Two Phase Flows and Heat Transfer, Proceedings of NATO Advanced Study Institute, 1976, pp. 1327–1346.
[18] L. Bolle, J.C. Moureau, Experimental study of heat transfer by spray cooling, in: D.B. Spalding, N.H. Afgan (Eds.), Heat and Mass Transfer in Metallurgical Systems, McGraw-Hill, New York, 1981, pp. 527–534.
[19] E.A. Mizikar, Spray-cooling investigation for continuous casting of billets and blooms, Iron Steel Eng. 47 (1970) 53–60.
[20] K. Sasaki, Y. Sugitani, M. Kawasaki, Heat transfer in spray cooling on hot surface, Tetsu-to-Hagane 65 (1979) 90–96.
[21] H. Mzad, M. Tebbal, Thermal diagnostics of highly heated surfaces using water-spray cooling, Heat Mass Transfer 45 (2009) 287–295.
[22] L. Ubanovich, V. Goryaninov, V. Sevost'yanov, Y. Boev, V. Niskovskikh, A. Grachev, A. Sevost'yanov, V. Gur'ev, Spray cooling of high-temperature metal surfaces with high water pressures, Steel in the USSR 11 (1981) 184–186.
[23] U. Reiners, R. Jeschar, R. Scholz, D. Zebrowski, W. Reichelt, A measuring method for quick determination of local heat transfer coefficients in spray cooling within the range of stable film boiling, Steel Res. 56 (1985) 239–246.
[24] R.A. Sharief, G.G. Nasr, A.J. Yule, Steady-state high-pressure spray cooling of high-temperature steel surfaces, Atom. Sprays 17 (2007) 171–191.
[25] J. Schmidt, H. Boye, Influence of velocity and size of the droplets on the heat transfer in spray cooling, Chem. Eng. Technol. 24 (2001) 255–260.
[26] Y. Ito, T. Murai, Y. Miki, M. Mitsuzono, T. Goto, Development of hard secondary cooling by high-pressure water spray in continuous casting, ISIJ Int. 51 (2011) 1454–1460.
[27] K.J. Choi, S.C. Yao, Heat transfer mechanisms of horizontally impacting spays, Int. J. Heat Mass Transfer 30 (1987) 1291–1296.
[28] L. Lin, R. Ponnappan, K. Yerkes, B. Hager, Large area spray cooling, in: 42nd AIAA Aerospace Sciences Meeting and Exhibit, AIAA, Reno, USA, 2004.
[29] K.-i. Yoshida, Y. Abe, T. Oka, Y. Mori, A. Nagashima, Spray cooling under reduced gravity condition, J. Heat Transfer – Trans. ASME 123 (2001) 309–318.
[30] S.C. Yao, K.J. Choi, Heat transfer experiments of mono-dispersed vertically impacting sprays, Int. J. Multiphase Flow 13 (1987) 639–648.
[31] B. Delcorio, K.J. Choi, Analysis of direct liquid-solid contact heat transfer in monodispersed spray cooling, J. Thermophys. Heat Transfer 5 (1991) 613–620.
[32] S. Deb, S.C. Yao, Heat transfer analysis of impacting dilute spray on surfaces beyond the Leidenfrost temperature, in: Proc. ASME National Heat Transfer Conference, ASME, Pittsburgh, USA, 1987, pp. 1–8.
[33] Y.-C. Kim, S. Nishio, H. Ohkubo, Spray cooling with formation of liquid film: distribution of heat-transfer coefficient in high-temperature region, Trans. JSME 60 (1994) 2158–2164.
[34] Y.-C. Kim, S. Nishio, H. Ohkubo, Spray cooling with formation of liquid film: film-boiling heat transfer of liquid film flow, Trans. JSME 62 (1996) 734–739.
[35] Y.-C. Kim, S. Nishio, H. Ohkubo, Experimental study on heat transfer in high temperature region of spray cooling interacting with liquid film flow, in: Proc. 3rd KSME-JSME Thermal and Fluid Engineering Conference Kyongju, Korea, 1996, pp. 243–248.
[36] S. Nishio, Y.-C. Kim, Heat transfer of dilute spray impinging on hot surface (simple model focusing on rebound motion and sensible heat of droplets), Int. J. Heat Mass Transfer 41 (1998) 4113–4119.
[37] H.M. Al-Ahmadi, S.C. Yao, Spray cooling of high temperature metals using high mass flux industrial nozzles, Exp. Heat Transfer 21 (2008) 38–54.
[38] S.-S. Hsieh, T.-C. Fan, H.-H. Tsai, Spray cooling characteristics of water and R-134a. Part II: Transient cooling, Int. J. Heat Mass Transfer 47 (2004) 5713–5724.
[39] J. Wendelstorf, K.-H. Spitzer, R. Wendelstorf, Spray water cooling heat transfer at high temperatures and liquid mass fluxes, Int. J. Heat Mass Transfer 51 (2008) 4902–4910.
[40] H. Fujimoto, N. Hatta, H. Asakawa, T. Hashimoto, Predictable modelling of heat transfer coefficient between spraying water and a hot surface above the Leidenfrost temperature, ISIJ Int. 37 (1997) 492–497.
[41] A. Moriyama, K. Araki, M. Yamagami, K. Mase, Local heat-transfer coefficient in spray cooling of hot surface, Trans. ISIJ 28 (1988) 104–109.
[42] S. Deb, S.C. Yao, Analysis on film boiling heat transfer of impacting sprays, Int. J. Heat Mass Transfer 32 (1989) 2099–2112.
[43] J.D. Bernardin, I. Mudawar, Film boiling heat transfer of droplet streams and sprays, Int. J. Heat Mass Transfer 40 (1997) 2579–2593.
[44] T.L. Cox, S.C. Yao, Heat transfer of sprays of large water drops impacting on high temperature surfaces, J. Heat Transfer – Trans. ASME 121 (1999) 446–456.
[45] S.C. Yao, T.L. Cox, A general heat transfer correlation for impacting water sprays on high-temperature surfaces, Exp. Heat Transfer 15 (2002) 207–219.
[46] T. Ito, Y. Takata, M.M.M. Mousa, H. Yoshikai, Studies on the water cooling of hot surfaces (experiment of spray cooling), Mem. Faculty Eng. Kyushu Univ. 51 (1991) 119–144.
[47] M. Shoji, T. Wakunaga, K. Kodama, Heat transfer from a heated surface to an impinging subcooled droplet (Heat transfert characteristics in the non-wetting regime), Heat Transfer-Jap. Res. 13 (1984) 50–67.
[48] A. Labergue, M. Gradeck, F. Lemoine, Comparative study of the cooling of a hot temperature surface using sprays and liquid jets, Int. J. Heat Mass Transfer 81 (2015) 889–900.
[49] A. Labergue, J.-D. Pena-Carillo, M. Gradeck, F. Lemoine, Combined three-color LIF-PDA measurements and infrared thermography applied to the study of the spray impingement on a heated surface above the Leidenfrost regime, Int. J. Heat Mass Transfer 104 (2017) 1008–1021.
[50] C.J. Hoogendoorn, R. den Hond, Leidenfrost temperature and heat-transfer coefficients for water sprays impinging on a hot surface, in: Proc. 5th International Heat Transfer Conference, Tokyo, Japan, 1974, pp. 135–138.
[51] B.S. Gottfried, C.J. Lee, K.J. Bell, The leidenfrost phenomenon: film boiling of liquid droplets on a flat plate, Int. J. Heat Mass Transfer 9 (1966) 1167–1188.
[52] N. Sozbir, Y.W. Chang, S.C. Yao, Heat transfer of impacting water mist on high temperature metal surfaces, J. Heat Transfer – Trans. ASME 125 (2003) 70–74.
[53] N. Sozbir, C. Yigit, R.J. Issa, S.-C. Yao, H.R. Guven, S. Ozcelebi, Multiphase spray cooling of steel plates near the Leidenfrost temperature-Experimental studies and numerical modeling, Atom. Sprays 20 (2010) 387–405.
[54] J.D. Bernardin, I. Mudawar, A Leidenfrost point model for impinging droplets and sprays, J. Heat Transfer – Trans. ASME 126 (2004) 272–278.
[55] J.D. Bernardin, I. Mudawar, A cavity activation and bubble growth model of the Leidenfrost point, J. Heat Transfer – Trans. ASME 124 (2002) 864–874.
[56] O.G. Engel, Note on particle velocity in collisions between liquid drops and solids, J. Res. Nat. Bur. Stand. A 64 (1960) 497–498.
[57] O.G. Engel, Waterdrop collisions with solid surfaces, J. Res. Nat. Bur. Stand. A 54 (1955) 281–298.
[58] D.D. Hall, I. Mudawar, Predicting the impact of quenching on mechanical properties of complex-shaped aluminum alloy parts, J. Heat Transfer – Trns. ASME 117 (1995) 479–488.
[59] D.D. Hall, I. Mudawar, R.E. Morgan, S.L. Ehlers, Validation of a systematic approach to modeling spray quenching of aluminum alloy extrusions, composites, and continuous castings, J. Mater. Eng. Perform. 6 (1997) 77–92.
[60] T.A. Deiters, I. Mudawar, Optimization of spray quenching for aluminum extrusion, forging, or continuous casting, J. Heat. Treat. 7 (1989) 9–18.
[61] T.A. Deiters, I. Mudawar, Prediction of the temperature-time cooling curves for three-dimensional aluminum products during spray quenching, J. Heat. Treat. 8 (1990) 81–91.
[62] I. Mudawar, T.A. Deiters, A universal approach to predicting temperature response of metallic parts to spray quenching, Int. J. Heat Mass Transfer 37 (1994) 347–362.

[63] J.C. Rozzi, W.P. Klinzing, I. Mudawar, Effects of spray configuration on the uniformity of cooling rate and hardness in the quenching of aluminum parts with nonuniform shapes, J. Mater. Eng. Perform. 1 (1992) 49–60.
[64] J.R. Rybicki, I. Mudawar, Single-phase and two-phase cooling characteristics of upward-facing and downward-facing sprays, Int. J. Heat Mass Transfer 49 (2006) 5–16.
[65] K.A. Estes, I. Mudawar, Correlation of Sauter mean diameter and critical heat flux for spray cooling of small surfaces, Int. J. Heat Mass Transfer 38 (1995) 2985–2996.
[66] D.D. Hall, I. Mudawar, Optimization of quench history of aluminum parts for superior mechanical properties, Int. J. Heat Mass Transfer 39 (1996) 81–95.
[67] D.D. Hall, I. Mudawar, Experimental and numerical study of quenching complex-shaped metallic alloys with multiple, overlapping sprays, Int. J. Heat Mass Transfer 38 (1995) 1201–1216.
[68] J.D. Bernardin, I. Mudawar, Experimental and statistical investigation of changes in surface roughness associated with spray quenching, Int. J. Heat Mass Transfer 39 (1996) 2023–2037.
[69] J.D. Bernardin, I. Mudawar, An experimental investigation into the relationship between temperature-time history and surface roughness in the spray quenching of aluminum parts, J. Eng. Mater. Technol. 118 (1996) 127–134.
[70] F.P. Buckingham, A. Haji-Sheikh, Cooling of high-temperature cylindrical surfaces using a water-air spray, J. Heat Transfer – Trans. ASME 117 (1995) 1018–1027.
[71] J.W. Hodgson, R.T. Saterbak, J.E. Sunderland, An experimental investigation of heat transfer from a spray cooled isothermal cylinder, J. Heat Transfer – Trans. ASME 90 (1968) 457–463.
[72] J.W. Hodgson, J.E. Sunderland, Heat transfer from a spray-cooled isothermal cylinder, Ind. Eng. Chem. Fundam. 7 (1968) 567–572.
[73] R.L. Mednick, C.P. Colver, Heat transfer from a cylinder in an air-water spray flow stream, AIChE J. 15 (1969) 357–362.
[74] N. Mascarenhas, I. Mudawar, Methodology for predicting spray quenching of thick-walled metal alloy tubes, Int. J. Heat Mass Transfer 55 (2012) 2953–2964.